Dynamics and interactions of highly resolved marine plankton via automated high frequency sampling

David M. Needham[1], Erin B. Fichot[1], Ellice Wang[1], Lyria Berdjeb[1], Jacob A. Cram[1], Cedric G. Fichot[2], Jed A. Fuhrman[1]

[1]Department of Biological Sciences, University of Southern California
[2]Earth and Environment, Boston University

Conflicts of Interest: The authors declare no conflict of interest.

Abstract

Short time-scale observations are valuable for understanding microbial ecological processes. We assessed dynamics in relative abundance and potential activities by sequencing the small sub-unit ribosomal RNA gene (rRNA gene) and rRNA molecules (rRNA) of *Bacteria*, *Archaea*, and *Eukaryota* once to twice-daily between March 2014 and May 2014 from the surface ocean off Catalina Island, California. Typically *Ostreococcus, Braarudosphaera, Teleaulax, and Synechococcus* dominated phytoplankton sequences (including chloroplasts) while SAR11, *Sulfitobacter,* and *Fluviicola* dominated non-phytoplankton *Bacteria* and *Archaea*. We observed short-lived increases of diatoms, mostly *Pseudo-nitzschia* and *Chaetoceros,* with quickly responding *Bacteria* and *Archaea* including *Flavobacteriaceae* (*Polaribacter* & *Formosa*), *Roseovarius,* and *Euryarchaeota* (MGII), notably the exact amplicon sequence variants we observed responding similarly to another diatom bloom nearby, three years prior. We observed correlations representing known interactions among abundant phytoplankton rRNA sequences, demonstrating the biogeochemical and ecological relevance of such interactions: 1) The kleptochloroplastidic ciliate *Mesodinium* 18S rRNA gene sequences and a single *Teleaulax* taxon (via 16S rRNA gene sequences) were correlated (Spearman r =0.83) yet uncorrelated to a *Teleaulax* 18S rRNA gene OTU, or any other taxon (consistent with a kleptochloroplastidic or karyoklepty relationship) and 2) the photosynthetic prymnesiophyte *Braarudosphaera bigelowii* and two strains of diazotrophic cyanobacterium UCYN-A were correlated and each taxon was also correlated to other taxa, including *B. bigelowii* to a verrucomicrobium and a dictyochophyte phytoplankter (all $r > 0.8$). We also report strong correlations ($r > 0.7$) between various ciliates, bacteria, and phytoplankton, suggesting interactions via currently unknown mechanisms. These data reiterate the utility of high-frequency time-series to show rapid microbial reactions to stimuli, and provide new information about *in-situ* dynamics of previously recognized and hypothesized interactions.

63 **Introduction**

64 Natural marine microbial communities, consisting of *Bacteria*, *Archaea*, and
65 *Eukaryota*, are diverse and dynamic. The interactions among microbial species and
66 their environment and between microbial species dictate how energy and nutrients
67 flow through the ocean [1,2]. Marine microbial communities are known to be
68 seasonally variable [3–5] and can show rapid responses to environmental variation,
69 such as stratification and pulses of nutrients [6,7]. Daily or diel-scale high-resolution
70 time-series are particularly useful for observing ecological responses to short-term
71 perturbations, such as phytoplankton blooms and interactions of organisms,
72 because whole microbial generation times are on the scale of a few days [5,8].
73 During phytoplankton blooms, microbial communities can vary in pronounced,
74 succession-like ways with dominant taxa shifting quickly [6,9], even on time scales
75 of one to several days [7,10].
76
77 Complex ecological interactions between microorganisms are prevalent in the ocean
78 [1]. Such interactions can be general, such as lineages of *Bacteria* that consistently
79 respond to increases in phytoplankton biomass and the organic matter produced by
80 such blooms [11]. However, many interactions appear to be species specific,
81 including direct microbe-microbe interactions, and can be observed at short
82 temporal scales [2]. Such interactions include grazing, cross-feeding, mutualism,
83 parasitism, symbiosis, or kleptochloroplasty (i.e., where a heterotrophic protist
84 captures chloroplasts from another species and the chloroplast continues to
85 function inside the grazer) [12]. Many of these interactions occur beween organisms
86 of different domains or trophic states, e.g., between *Bacteria* and *Eukaryota*, or
87 between phototrophs and heterotrophs. Studying all of these organisms together
88 allows a more complete view of components in the "microbial loop" [13].
89
90 The dynamics and ecology of microbial organisms via time-series is often assessed
91 via sequencing of the small subunit ribosomal rRNA gene of cellular organisms,
92 which is conserved across all three domains of life. We have recently shown that a
93 single rRNA gene primer set has high coverage of *Bacteria* and *Archaea*, most

94 phytoplankton via chloroplast 16S rRNA gene sequencing, as well as covering most
95 *Eukaryota* via 18S rRNA gene sequencing [7,14]. With current sequencing outputs
96 from the Illumina MiSeq and HiSeq platform (paired end 2x250 or 2x300 high
97 quality reads), it is possible to confidently discriminate taxa by as little as a single
98 base pair (bp) difference in this conserved gene, which is the highest resolution
99 possible for this method [15–17], but this often, still, does not reliably discriminate
100 strains or even species.
101
102 A complementary approach to sequencing the rRNA gene is reverse transcribing
103 and sequencing of the small sub-unit of the rRNA molecule itself (rRNA) which
104 provides the same identity information as DNA, but the number of sequences is
105 considered a proxy for the cumulative number of ribosomes from that taxon. The
106 approach may yield insight into the potential activities of taxa across the full
107 community [18–21]. The rRNA and rRNA gene sequencing approaches each have
108 benefits and uncertainties. First, in any PCR-based approach, choice of primer
109 influences the result and can bias against certain taxa. Though, we have shown that
110 the primers recreate known inputs, i.e., mock communities, reasonably accurately,
111 some taxa are still biased for or against and some groups may be missed. For the
112 rRNA gene, while the gene copy number in the genome varies between taxa, it is
113 relatively consistent within individuals of a given taxon and across time. The large
114 majority of free living planktonic marine *Bacteria* and *Archaea* have 1-2 copies per
115 cell [22]. For chloroplasts, copy number is usually between 1-2 per chloroplast,
116 while the number of chloroplasts per cell can vary from one to hundreds (depending
117 largely on cell size [7]). However, for small phytoplankton most commonly found
118 offshore of Southern California, USA (the location of the present study), the variation
119 is typically low (two to four chloroplasts for common taxa)[7]. The 18S rRNA gene
120 of *Eukaryota*, on the other hand, has a larger range in copy number, from 2 to 50,000
121 [23]. Thus, comparing relative abundances for these taxa via 18S rRNA gene is
122 tenuous, but the copy number variation relates very roughly to cellular biomass,
123 when compared over many orders of magnitude on a log-log plot [23]. rRNA, in
124 contrast, may in part reflect variation of "potential activity" between and within taxa

125 over time. However, the number of ribosomes per cell does not consistently reflect
126 growth rate across taxa, because the relationship is irregular between taxa, and it is
127 not anything like a linear measure of growth rate [20,21]. Previous work has
128 assessed the ratio between the rRNA and rRNA gene of individual taxa. Such work
129 reports an "index" that aims to examine the relative activities across taxa and
130 describe patterns across all taxa. Such an analysis, with all its inherent complexities
131 and complicating factors, is outside the scope of this paper.
132
133 Here we apply rRNA and rRNA gene sequencing to study the full cellular microbial
134 community -- *Bacteria*, *Archaea*, and *Eukaryota* -- from seawater samples collected
135 from the photic zone once to twice per day over about 1.5 months via an
136 Environmental Sample Processor (ESP), which also provided continuous physical
137 and chemical measurements. We examined the short-term dynamics of the
138 microbial community before and after a short-lived increase in phytoplankton
139 biomass. Additionally, we found that the members of two symbioses were prevalent
140 during our time-series: 1.) the ciliate *Mesodinium* and the chloroplasts of the
141 cryptophyte *Teleaulax* [24] and 2.) the diazotrophic cyanobacterium UCYN-A and
142 haptophyte alga *Braarudosphaera bigelowii* [25]. This allowed us to assess the *in-*
143 *situ* relative abundances and physiological dynamics of these relationships, which
144 provides insight into the nature of these associations. We also explore other strong
145 co-occurrence patterns between phytoplankton, potential eukaryotic grazers,
146 bacteria, and archaea to examine potential new interactions.
147
148 **Methods**
149 **Sampling**
150 An Environmental Sample Processor (ESP) [26], which autonomously draws
151 seawater samples and filters them sequentially while also recording depth,
152 temperature, conductivity, and chlorophyll-*a* fluorescence was deployed about 1 km
153 offshore of Santa Catalina Island, California, USA (33 28.990 °N, 118 30.470 °W) 13
154 March 2014 to 1 May 2014. The ESP was tethered to the sea floor by a long cable, in
155 a location of about 200 m total water depth, and thus sampled in Eulerian fashion.

The depth at which the instrument itself was suspended in the water column varied over the course of a day, due to tides and tidal currents. Over the first five days, the depth of sampling by the instrument was between 5 and 10 m. The ESP malfunctioned on day six. After the instrument was restored two weeks later, samples were collected by the instrument at depths between 7 m and 15 m (Figure 1), which continued throughout the remainder of the time-series. One L water samples for molecular analysis were drawn once (10 AM, 18 March to 23 March) or twice per day (10 AM and 10 PM, 9 April to 1 May). The samples were pre-screened with a 300 μm copper screen and then sequentially collected on a 1 μm AE filter (Pall Gelman) and a 0.22 μm Durapore filter (Millipore) with an HA backing filter. All filters were stored in RNAlater at ambient seawater temperature until ESP retrieval (1 May), upon which the filters were stored at -80 °C until processing. Past ESP research has demonstrated that RNAlater storage has little influence on quality and composition of RNA for ESP deployments (6 of 17,284 transcripts differentially expressed) [27], but RNAlater has been shown, like all preservatives, to have a small influence on composition based on DNA-based community assessments[28,29], though the influence was not tested here.

The ESP recorded depth, temperature, conductivity, and chlorophyll-*a* fluorescence measurements every five minutes. Reported tidal heights are from the National Oceanographic and Atmospheric Administration's observed water heights for a Los Angeles, CA, USA station (9410660) which is about 35 km from where the ESP was deployed (https://tidesandcurrents.noaa.gov).

Satellite imagery

Level-2 remote-sensing reflectances (*Rrs*) from *Aqua* MODIS (MODerate Resolution Imaging Spectrometer) were used to produce daily maps of surface chlorophyll-*a* concentrations over the 1 March 2014 - 30 April 2014 time period. About one third of all the images were discarded because of cloud coverage. The surface chlorophyll-*a* concentrations were derived by applying a local empirical algorithm to the *Rrs*(488)/*Rrs*(547) remote-sensing reflectance ratio [30]. This local empirical

187 algorithm was parameterized specifically for MODIS using *in situ* measurements
188 made in the coastal waters off the Los Angeles, CA area (i.e., our region of study). A
189 time-series of remotely sensed chlorophyll-*a* concentration at the ESP location was
190 also calculated by averaging the retrievals over a ~ 3-x-3 km region (i.e., 3-x-3
191 pixels) surrounding the ESP location, and by calculating the standard deviation of all
192 retrievals within that region. Only the chlorophyll-*a* concentrations derived from a
193 minimum of seven valid pixels within the 3-x-3-pixels region were considered, as
194 fewer valid pixels generally indicated the close proximity of clouds and a potential
195 contamination of the remote-sensing reflectances.
196
197 **DNA and RNA extraction**
198 Each AE and Durapore filter was aseptically cut in half, one half for DNA extraction,
199 the other half for RNA extraction. DNA was extracted and purified from the
200 Durapore filters using a hot SDS extraction protocol [31] and from the AE filters
201 using a NaCl/cetyl trimethylammonium bromide (CTAB) bead-beating extraction
202 [32]. The more harsh extraction used on the larger size fraction was used to contend
203 with the organisms found on the larger size fraction are harder to break open (e.g.,
204 algal cell walls, diatom silica frustules, and dinofagellate theca). Each of these
205 methods was modified to include lysozyme and proteinase K lysis steps (30 minutes
206 at 37 °C and 30 minutes at 50 °C, respectively). DNA was purified from the
207 supernatant from both methods by phenol/chloroform/isoamyl alcohol purification,
208 precipitation overnight in ammonium acetate and ethanol, centrifugation, and re-
209 suspension in TE buffer. Each half-filter underwent two sequential lysis steps, and
210 the extracted DNA was combined.
211 RNA was extracted from the Durapore and AE filter using the RNeasy kit (Qiagen),
212 as per manufacturer's instructions, including an on-column DNAse step. For the AE
213 filters, a second DNA-removal step was performed on 10 ng of RNA with the
214 Invitrogen DNAse I, Amplification Grade (Cat. Number: 18068015).
215 **Reverse transcription and PCR**
216 RNA was reverse transcribed to cDNA using SuperScript III from Invitrogen using
217 random hexamers, with 0.1 ng for the Durapore size fraction and all of the RNA from

218 the Invitrogen DNAse treated AE RNA (input 10 ng). cDNA was purified
219 magnetically with 2x Ampure beads. Cleaned cDNA was then amplified for 30 cycles
220 via PCR with 5PRIME HotMasterMix. The forward SSU rRNA primer construct
221 consisted of (5' to 3') a 'generic' Illumina flow cell adapter, Illumina sequencing
222 primer, 4 random bp, five base barcode, and SSU rRNA gene forward primer 515F
223 (GTGYCAGCMGCCGCGGTAA). Reverse primer construct consisted of (5' to 3') a
224 'generic' Illumina flow cell adapter, 6 bp index, sequencing primer, and rRNA
225 reverse primer 926R (CCGYCAATTYMTTTRAGTTT) [7,14]. Thermocycling
226 conditions consisted of an initial denaturation of 95 °C for 120 s; 25 cycles of 95 °C
227 for 45 s, 50 °C for 45 s, 68 °C for 90 s; and a final elongation step 68 °C for 300 s
228 [7,14]. We concluded that RNA extracts were devoid of significant DNA by
229 performing no-RT PCR and observing an absence of amplification in an agarose gel.
230 DNA from Durapore (0.5 ng) and AE filters (0.05 ng) was amplified by 30 and 35
231 cycles, respectively. For the AE DNA PCR amplifications, five extra PCR cycles and
232 10-fold reduced DNA template were necessary because of (presumably) an
233 inhibitory effect of the RNAlater on the extracted DNA. After PCR, products were
234 cleaned and concentrated with Ampure beads and pooled. All samples were
235 sequenced in one MiSeq 2x300 run at University of California, Davis.
236 **Sequence Analysis**
237 All commands run during data analysis and figure generation are available via
238 Figshare (10.6084/m9.figshare.5373916). Sequences are available via EMBL study
239 accession number PRJEB22356. Demultiplexed samples were trimmed via a sliding
240 window of 5, trimming where the window average quality dropped below q20 via
241 Trimmomatic. Sequences less than 200 bp were removed. For 16S rRNA and rRNA
242 gene analysis, forward and reverse reads were then merged with a minimum
243 overlap of 20 bp, minimum merged length of 200 bp and maximum differences (in
244 overlap region) of 3 bp using USEARCH [33]. Both 18S rRNA and rRNA gene
245 sequence forward and reverse reads did not overlap so this merging step retains
246 only 16S rRNA and rRNA gene sequences. A separate analysis was necessary for the
247 18S rRNA and rRNA gene sequence (see below). Primers were removed from the
248 sequences with cutadapt [34]. Chimeras were detected *de novo* and reference-based

249 searching with QIIME *identify_chimeric seqs.py* and with the SILVA gold database
250 [35] as the reference [36]. Merged 16S rRNA and rRNA gene sequences were then
251 padded to make them all the same length with *o-pad-with-gaps* via the *Oligotyping*
252 pipeline [37]. Then the sequences were "decomposed" with Minimum Entropy
253 Decomposition (MED) default settings [15]. MED decomposes the sequences into
254 types that are distinguished by as little as a single base, based on an assessment of
255 the underlying sequence variability and positions of high variability. We recently
256 concluded that this approach performs well for our assays via custom-made marine
257 mock communities [10]. We refer to these highly resolved sequences as Amplicon
258 Sequence Variants (ASVs).
259
260 Sequence classification was performed on representative sequences from the 16S
261 rRNA and rRNA gene ASVs via SILVA [35], Greengenes [38], and PhytoREF [39]
262 databases using UCLUST [40] via the QIIME *assign_taxonomy.py* command. The
263 PhytoREF database was used for classification of chloroplast 16S rRNA and rRNA
264 gene sequences. Additionally we also searched the sequences for cultured relatives
265 in the NCBI nr database (see Needham and Fuhrman 2016 for details) with BLASTn
266 [41]. All classifications and representative sequences are available via Figshare
267 (Public Project Link: https://goo.gl/nM1cwe). For the 16S rRNA and rRNA gene
268 non-phytoplankton sequences, we generally display the SILVA and Phytoref for the
269 non-phytoplankton and phytoplankton, respectively. However, in some cases, we
270 used matches from NCBI because the more curated databases (e.g., SILVA) may lack
271 the most up-to-date sequences available. We generally confirmed the NCBI
272 classifications via phylogenetics (e.g., UCYN-A, see below).
273
274 We performed manual curation of our classification in the following cases: 1.)
275 *Prasinophyceae* sequences were all manually curated because an abundant
276 *Prasinophyceae* sequence was initially annotated as *Ostreococcus* and *Bathycoccus*
277 via the NCBI and Phytoref databases, respectively. By manual inspection, we found
278 that the ASV perfectly matched an *Ostreococcus* genome sequence; we updated the
279 classification throughout the manuscript (Supplementary Figure 1). 2.). We found

280 that UCYN-A sequences are generically classified by the SILVA database as
281 Cyanobacterial Subsection I, Family I (i.e., same groups as to *Prochlorococcus* and
282 *Synechococcus*). To resolve the UCYN-A sequences to their respective sub-groups we
283 downloaded the sequences of UCYN-A1 [42] (gi|284809060) and UCYN-A2
284 [43](gi|671395793). We found the UCYN-A1 and UCYN-A2 rRNA gene sequences
285 from these genomes were 3 bp different in the V4 to V5 amplified region we used
286 (i.e., 99.2% similar). Each of our two UCYN-A ASVs matched one of each of the
287 representative genomes at 100% (Supplementary Figure 2), thus we notated them
288 accordingly.
289
290 We split the 16S rRNA and rRNA gene sequence datasets into two partitions, the
291 "phytoplankton" and "non-phytoplankton." "Phytoplankton" included those
292 sequences determined by the Greengenes taxonomy to be of chloroplastidic origin
293 and *Cyanobacteria*. "Non-phytoplankton" included the remaining bacterial and
294 archaeal 16S rRNA and rRNA gene sequences. After this step, samples that did not
295 have greater than 100 reads in a given dataset were removed from further analysis.
296 The average number of reads per sample for non-phytoplankton and phytoplankton
297 datasets was 16,576 ± 9,302 SD and 13,426 ± 11,478 SD, respectively.
298
299 The 18S rRNA and rRNA gene forward and reverse sequencing reads were too long
300 to overlap, given the MiSeq 2x300 forward and reverse sequencing that we used.
301 Therefore, most programs that merge forward and reverse reads discard these
302 reads. Hence, they need special treatment. The following steps were taken to
303 process these data. 1.) The data were quality filtered the same as for the 16S rRNA
304 and rRNA gene analysis via Trimmomatic. 2.) The resulting quality filtered forward
305 and reverse reads were trimmed to 290 bp and 250 bp, respectively. Reads that
306 were shorter than those thresholds were discarded. The sequences were trimmed to
307 these different lengths due to the difference in read qualities between the forward
308 and reverse reads (forward is higher quality). Given these trimmed sequence
309 lengths, the 16S rRNA and rRNA gene reads will overlap but the 18S rRNA and rRNA
310 gene reads will not. 3.) We collected the 18S rRNA and rRNA gene reads by running

311 all the reads through PEAR merging software [44], using default settings, and
312 retained the unassembled reads. 4.) The forward and reverse reads of the
313 unassembled reads were then joined with a degenerate base, "N", between the two
314 reads. This approach was suitable for classification via 8 bp subsequences ("words"
315 or "kmers") - based RDP classifier [45,46] as well as a local alignment-based tool
316 such as BLAST. Due to relatively low numbers of 18S rRNA and rRNA gene
317 sequences (646 ±403 SD reads per sample), we did not perform MED, but clustered
318 the sequences into OTUs at 99% sequence similarity via QIIME *pick_otus.py*, using
319 the UCLUST option. We chose the OTU approach because MED relies upon relatively
320 high coverage to help confidently differentiate between sequencing errors and true
321 variants. 18S rRNA and rRNA gene sequence OTU representative sequences were
322 classified with *assign_taxonomy.py* via the RDP classifier option against the Protistan
323 Ribosomal Reference (PR2) database and SILVA database, and against the NCBI
324 database as previously described using BLASTn. We generally used the PR2
325 classifications. All classifications and representative sequences are available via
326 Figshare (https://goo.gl/nM1cwe). For the 18S rRNA and rRNA gene sequence data,
327 we generally report the data as proportions of non-metazoan 18S rRNA and rRNA
328 gene sequences, except where specified.
329
330 Phylogenetic trees were generated for the most abundant unique sequence from the
331 ASVs (16S rRNA gene sequences) and OTUs (18S rRNA gene sequences) with
332 MUSCLE default settings with a maximum of 100 iterations [47]. Phylogenies were
333 reconstructed using PhyML default settings [48]. Notably, in the 18S rRNA gene tree,
334 *Mesodinium* is divergent from the rest of the ciliates due to a very aberrant 18S
335 rRNA gene sequence which has been previously reported [49].
336
337 **Statistical Analysis**
338 Pairwise correlations between parameters were performed using eLSA [50,51]. To
339 focus networks on the most prevalent taxa, only ASVs and OTUs that met the
340 following thresholds for each given dataset were considered: 1.) detected in 75% of
341 samples, 2.) a mean relative proportion greater than of 0.05%, and 3.) a relative

342 proportion of greater than 0.5% for at least one day. Missing data were interpolated
343 linearly (typically only a few samples per dataset, except for 18S rRNA which had 12
344 (of 53) days missing), and p and q values were determined via a theoretical
345 calculation [51]. Due to the two weeks of missing data, we did not consider time-
346 lagged correlations. Only correlations that had p and $q < 0.005$ were considered
347 significant. Due to the large variation in number of pairwise correlations for some
348 associations versus others (phytoplankton and non-phytoplankton versus
349 eukaryotes to non-phytoplankton), we use different Spearman correlation values in
350 different network figures (but always with p and $q < 0.005$ and at $r > |0.70|$). For
351 Figure 7, where we display correlations to "heterotrophic taxa of *Eukaryota*", we
352 excluded lineages of *Eukaryota* that contain completely phototrophic taxa
353 (*Chlorophyta*, *Archaeplastida*, Stramenopiles, and *Haptophyta*). Note, removing all
354 Stramenopiles from the analysis, also removed "MAST" groups, which may be
355 primarily heterotrophic. Other network-specific details regarding the taxonomic
356 groups considered for a given network are displayed either within figure legends or
357 figure headings.
358
359 Mantel tests were performed in R [52] via vegan package's [53] "mantel" calculation,
360 on a fully overlapping dataset of 41 samples. We excluded the 18S rRNA dataset
361 from this analysis because this dataset was missing many samples relative to the
362 other datasets due to low read counts. Additionally, we avoided using the smaller
363 size fraction (0.22-1 μm) phytoplankton rRNA and rRNA gene sequences for
364 statistical associations. This is because most phytoplankton taxa are not observed in
365 this fraction. However, the smaller phytoplankton do typically appear in the 1-300
366 μm size fraction. Thus, this size fraction is likely a more meaningful representation
367 of the phytoplankton community.
368
369 **Results and Discussion**
370 Over the initial six days of sampling, conditions at the sampling location, 1 km off
371 Catalina Island, CA, USA, were relatively stable, with chlorophyll-*a* concentrations of
372 0.5-1.5 μg/L (Figure 1). After the 6th sample, the ESP malfunctioned. During a 15-day

373 non-operational period, satellite data indicated that a modest increase (about
374 fourfold background levels) in chlorophyll-*a* concentration (indicative of
375 phytoplankton biomass) occurred throughout the San Pedro Channel. The increase
376 in phytoplankton biomass started near the Southern Californian coast (to the
377 northwest of the ESP deployment location) and then extended towards the sampling
378 location near Catalina Island, with the highest concentrations reaching closest to the
379 location of the ESP four days before the instrument was repaired and sampling
380 continued (Figure 1, Supplementary Figure 3). When sampling resumed, the
381 chlorophyll-*a* concentrations were still elevated (though below peak levels
382 according to satellite data) and remained between 1-5 μg/L for the remainder of the
383 time-series. We noted cyclical patterns within the chlorophyll-*a* data, apparently
384 reflecting a combination of diel phytoplankton migrations and physiological
385 variations [54] and depth variations due to changes in tidal height and tidal currents
386 moving the instrument laterally (Figure 1).
387
388 *Overall community dynamics*
389 We performed sequencing of the small sub-unit of rRNA and rRNA gene sequences
390 of *Archaea*, *Bacteria*, and chloroplasts, as well as 18S rRNA and rRNA gene
391 sequences of *Eukaryota*. A major consideration is how to partition this data into
392 ecologically relevant communities. In this study, we partitioned the 16S rRNA and
393 rRNA gene sequences into two groups: 1.) "phytoplankton" (chloroplast sequences
394 and *Cyanobacteria*, i.e., the "primary producers") and 2.) "non-phytoplankton" (all
395 other *Bacteria* and *Archaea*, assumed here, for simplicity sake, to be largely
396 heterotrophic, i.e., the "secondary consumers"). Certainly, divisions between these
397 classically defined trophic levels are recognized as being "fuzzy," including the
398 common occurrence of various types of mixotrophs [1]. However, this approach was
399 taken because it allows a more independent assessment of the influence of the
400 major primary producer communities (in the surface ocean, phytoplankton) on the
401 secondary consumers, in a manner that combining the *Cyanobacteria* with the other
402 *Bacteria* and *Archaea* does not allow. Additionally, a complicating factor of primary
403 versus secondary producers is the fact that many bacteria and archaea have

404 phototrophic capability via proteorhodopsin [55] or bacteriochlorophyll [56,57],
405 and some are chemoautotrophs (e.g., *Thaumarchaeota* [58]). An obvious
406 consideration of including the *Cyanobacteria* in the same data partition as the
407 chloroplasts is that, on a cell-by-cell basis, chloroplast rRNA gene sequence will be
408 overrepresented relative to their true cellular abundances. This is because
409 cyanobacteria have a maximum of two rRNA gene copies per cell, whereas protists
410 can have many chloroplasts. Regardless of how the data are partitioned, at this
411 broad taxonomic level, differences in the biology, copy number, and PCR
412 amplification bias are unavoidable and thus a direct one-to-one relationship of the
413 read sequence proportions to biomass or cell numbers from sequence data is not
414 possible. However, relative changes in read proportions of taxa over the course of
415 two months at diel to daily time scales are expected to be ecologically informative.
416
417 Due to the difficulty of accurately predicting the primary lifestyle of many
418 eukaryotic taxa determined by 18S rRNA and rRNA gene sequences, the ability of
419 many protists to be mixotrophic [12], and because of the unknown presence of
420 chloroplasts in some lineages, we generally analyzed all of the *Eukaryota* rRNA and
421 rRNA gene OTUs as proportion of all *Eukaryota*, excluding only metazoan sequences.
422 Metazoan sequences appeared in the data sporadically and because their especially
423 high 18S rRNA gene copy number and multi-cellularity likely strongly biases the
424 data. Thus, we generally excluded metazoan sequences (e.g., copepods) because
425 their inclusion would alter the interpretation of a primary focus, the microbial
426 eukaryotes.
427
428 At the broadest level, the 16S rRNA gene sequences tended to be from non-
429 phytoplankton taxa, especially in the smaller size fraction, averaging 58% of the
430 total in the large size-fraction (1-300 μm) and 85% in the smaller size-fraction (0.22
431 – 1 μm)(Figure 2). Phytoplankton made up the majority of the rest of the rRNA gene
432 relative proportions, 39% and 15%, respectively, of the large and small size
433 fractions. 18S rRNA gene sequences made up 3.6% and 0.1% in the large and small
434 fractions, respectively. These values provide an overall view of the read frequencies

435 that can be expected from our "universal" sequencing approach, but they do not
436 provide insight into overall cell number or biomass of these partitions, where flow
437 cytometry or microscopy would be more useful. Additionally, because the data are
438 compositional, meaning always a proportion of 100%, a decrease in one partition of
439 the data necessarily results in an increase in another partition, even when there may
440 have been no absolute response in the latter. This also applies to individual ASV
441 relative abundances.
442
443 In contrast to the rRNA gene, the relative proportion of phytoplankton rRNA was
444 higher than non-phytoplankton rRNA in the larger size fraction (65% and 35%,
445 respectively). In the smaller size fraction, the proportions of non-phytoplankton and
446 phytoplankton rRNA were of roughly equal proportion (averages of 53% and 43%,
447 respectively), with the exception of following the phytoplankton bloom when non-
448 phytoplankton made up >95% of the rRNA sequences in the small size fraction for
449 several sampling dates (Figure 2). In both size fractions, 18S rRNA always
450 constituted less than 10% of the total reads, and were almost always negligible in
451 the small size fraction (Figure 2). Thus, the rRNA sequence frequencies from the
452 different partitions are variable depending on size fraction and environmental
453 conditions, but we do not know the extent that this relates to relative community
454 activities, given the major differences in biology between the partitions.
455
456 *Dynamics of individual phytoplankton taxa*
457 Within the phytoplankton community, the *Synechococcus* ASVs tended to have the
458 highest read proportions in both rRNA and rRNA gene, in both size fractions (Figure
459 3). In the larger size fraction, one of two different *Synechococcus* ASVs were the
460 highest in read proportions in 24 and 44 of 50 days in rRNA gene and rRNA,
461 respectively. In the smaller size fraction, a single *Synechococcus* ASV was dominant
462 in all 47 rRNA gene sequenced samples, and in 52 of 53 of the rRNA sequenced
463 samples, with a *Prochlorococcus* ASV exceeding it on a single date in rRNA.
464

465 Besides *Synechococcus*, in the larger size fraction, a variety of eukaryotic
466 phytoplankton ASVs (via chloroplasts) were found to display the highest sequence
467 proportion among all phytoplankton ASVs for at least one sample within the time-
468 series in either the rRNA or rRNA gene-based analyses. This included ASVs of
469 *Ostreococcus* (14 days), *Teleaulax* (6 days), *Chrysochromulinaceae* (5 days),
470 *Braarudosphaera* (three days), and *Pseudo-nitzschia* (1 day) (Figure 3). Several
471 diatom ASVs, mostly *Chaetoceros* sp. and *Pseudo-nitzschia* sp., peaked in their
472 sequence proportions for a few days following the small phytoplankton biomass
473 increase (deduced from satellite chlorophyll-*a* measurements), which was likely
474 already decreasing by the time we resumed sampling (Supplementary Figure 4).
475 Pico-eukaryotic phytoplankton taxa (i.e., *Bathycoccus*, *Micromonas*, and
476 *Ostreococcus*) increased in relative read proportions steadily over the second half of
477 the time-series, and ultimately were the second and third most represented ASV in
478 the phytoplankton rRNA gene dataset on average (Supplementary Figure 4). In
479 addition, two ASVs of the diazotrophic, symbiotic unicellular cyanobacterium UCYN-
480 A were cumulatively 1.1% and 5.6% of sequences in the large size-fraction rRNA
481 gene and rRNA, respectively. UCYN-A constituted up to 25% of all rRNA
482 phytoplankton sequences in that size fraction (more detail below) (Supplementary
483 Figure 4). This observation of high rRNA and rRNA gene presence of UCYN-A in a
484 productive upwelling region is significant from an oceanographic standpoint
485 because they may be an important source of bio-available nitrogen (via nitrogen
486 fixation) in these surface waters even during spring and accompanying increases in
487 phytoplankton biomass. These observations and short-term dynamics complement
488 the previously documented activity of UCYN-A at this location throughout the year
489 where they were reported as particularly active in summer and winter [59].
490
491 In the smaller size fraction, besides *Cyanobacteria*, *Ostreococcus*, *Micromonas*,
492 *Bathycoccous*, and *Pelagomonas* were commonly high in sequence proportions
493 (Supplementary Figure 4). It appears that these taxa tended to be equally split
494 between both size fractions, with the exception of *Pelagomonas*, which had a higher
495 proportion in the small size fraction. Generally, *Cyanobacteria* tended to be a higher

496 proportion in the rRNA than rRNA gene, while the opposite was the case for the
497 eukaryotic phytoplankton in the small size fraction. It is unclear how much this
498 relates to the relative activities of the two groups, considering the likely major
499 differences in cellular physiology across domains.
500
501 *Dynamics of individual non-phytoplankton taxa*
502 Generally, a single SAR11 ASV had the highest rRNA gene sequence proportions of
503 the non-phytoplankton bacterial and archaeal communities in the small size fraction
504 (most abundant on 44 of 47 samples). In contrast, a variety of ASVs were observed
505 to make up the highest proportion of the sequences for at least one date in the larger
506 size fraction. In the rRNA gene sequences from the larger size fraction, the
507 dominance shifted between *Fluviicola* (24 days), *Roseovarius* (12), *Polaribacter* (3),
508 *Roseibacillus* (3), *Puniceicoccaceae* (*Verrucomicrobia*) (1), and Marine Group II
509 *Euryarchaeota* (1). For the rRNA, in both the smaller and larger size fractions, the
510 ASVs with highest proportions on a given day shifted among 11 and 10 different
511 taxa, respectively. We observed particularly rapid dynamics following the increase
512 in phytoplankton biomass (8 April – 13 April, Figure 3). For the large size fraction,
513 the same ASVs tended to be highest in read proportions in both the rRNA and rRNA
514 gene sequence datasets.
515
516 Previously, we reported on a larger diatom bloom that occurred three years earlier
517 at a location about 20 km away [7,10]. We also had daily resolved data for this time-
518 series. For that study we generated 99% OTUs and then discriminated ASVs within
519 the abundant OTUs (i.e., > 2.5% relative abundance on any given day, or 0.4% on
520 average). Overall, 119 of the 279 bacterial and archaeal ASVs that we report in the
521 present study were also reported in that previous study. For the present study, 15 of
522 the 20 ASVs that ever had the highest proportion of sequences across all samples
523 were also among the ASVs in the previous study. Several of the ASVs became most
524 relative abundant for at least one sample in both time-series: members of
525 *Flavobacteraceae* (*Polaribacter* and *Formosa*), *Verrucomicrobia* (*Roseibacillus* and
526 *Puniceicoccaceae*) Marine Group II *Euryarchaeota*, *Roseovarius*, and SAR11. The

527 rapid day-to-day variation in the 8 – 12 April period is similar to what we observed
528 previously, and the same ASVs of *Polaribacter*, *Roseibacillus*, and Marine Group II
529 *Euryarchaeota* became most abundant in response to increases in chlorophyll-*a*,
530 while *Roseovarius*, *Puniceicoccaceae*, and SAR11 peaked during more stable
531 conditions. However, the response here was not as pronounced as in 2011. In that
532 study, based on estimates from satellite imagery, the peak in chlorophyll-*a*
533 concentration was about fourfold larger. Thus, the 2011 bloom likely corresponded
534 to a larger release of organic material. The consistency between years of
535 phytoplankton bloom response, even among exact sequence variants, is similar to
536 those reported from the North Sea [60].
537
538 Often, particular ASVs were observed within both size fractions, but in the smaller
539 size fraction, their temporal variation and overall relative abundances were reduced
540 due to the sustained high relative abundance of SAR11 ASVs (cumulatively 23% and
541 30% in the rRNA and rRNA gene in 0.2-1 μM, respectively versus 2% and 6% in the
542 1-300 μm size fraction). Besides SAR11, other non-photosynthetic taxa that were
543 relatively higher in the smaller fraction were SAR92 and SAR86 of
544 *Gammaproteobacteria*, and OCS116 of *Alphaproteobacteria*, (Figure 3,
545 Supplementary Figure 5). Notably a *Vibrio* ASV peaked up to 30% in rRNA
546 sequences and 2% in rRNA gene sequences. This is surprising considering that
547 *Vibrios* are typically thought to be "bloom-responders" [11] but here had high rRNA
548 proportions before the bloom.
549
550 *Dynamics of individual eukaryotic taxa via 18S rRNA and rRNA gene sequences*
551 The eukaryotic community (1-300 μm) via 18S rRNA and rRNA gene sequences was
552 often dominated by metazoans, such as herbivorous copepods (*Paracalanus*) and
553 larvaceans (*Oikopleura*, which can graze particles as small as bacteria). A single
554 copepod OTU (*Paracalanus* sp.) was the most represented in the rRNA gene on 34 of
555 50 samples and larvacean OTU (*Oikopleura dioica)* being most represented on 16 of
556 44 dates in the rRNA (Supplementary Figure 6). Excluding metazoans, we observed
557 20 different *Eukaryota* OTUs which became the highest in sequence proportions for

558 a given sample via rRNA gene, including 21 samples by ciliates (10 samples by
559 *Mesodinium*), 11 samples by chlorophytes (*Ostreococcus* (4), *Bathycoccus* (5),
560 *Micromonas* (2)), and 9 samples by dinoflagellates (primarily *Gyrodinium* and
561 *Gymnodinium* four and two samples, respectively) (Figure 3, Supplementary Figure
562 7). Similarly, ciliates were typically the highest in sequence proportions in the rRNA
563 (29 of 44 days). However, in contrast to the rRNA gene, Stramenopiles were
564 commonly the highest in sequence proportions (14 of 44 dates) in the rRNA. As
565 suggested by this high variability, Bray-Curtis community similarity across samples
566 showed that the eukaryotic community via 18S rRNA and rRNA gene sequences was
567 more variable than the 16S rRNA and rRNA gene sequences of bacteria, archaea, and
568 phytoplankton (Supplementary Figure 8). This is despite the fact that the 18S rRNA
569 and rRNA gene datasets were assessed using less resolving OTU-based approach
570 rather than the MED-based approach for the 16S rRNA and rRNA gene datasets. The
571 reasons that the dominance patterns vary between rRNA and rRNA gene are
572 probably a combination of copy number differences and levels of activity, even given
573 that dormant cells have a baseline level of rRNA [20].
574
575 **Correlations between taxa**
576 Previously most marine microbial community pairwise correlative analyses have
577 been between the abundance of organisms irrespective of activity [2]. However for
578 many types of microbial interactions, it would be valuable to consider some
579 indicator of activity level of the organisms as well. We aimed to do so here by
580 including rRNA in addition to the rRNA gene relative abundances in the co-
581 occurrence patterns between taxa. We first examined known two-organism
582 symbiotic interactions that occur among abundant taxa within our samples. Then,
583 we examined the strong correlations across all taxa to identify possible interactions
584 among and between domains, such as syntrophy, symbiosis, or grazing.
585
586 *UCYN-A and Braarudosphaera*
587 A widely distributed and important group of cyanobacterial nitrogen fixers,
588 commonly known as UCYN-A, has a greatly reduced genome and metabolic

589 deficiencies that are evidently met by having a symbiotic relationship with algae
590 [25,61–63]. At least four types of UCYN-A have been reported (denoted UCYN-A1,
591 A2, A3, and A4) and these types likely vary in their hosts [61]. The most well-
592 supported UCYN-A symbiosis is a relationship between UCYN-A2 and the
593 haptophyte alga *Braarudosphaera bigelowii* [25,61,62]. Other UCYN-A types are
594 thought to be associated with different phytoplankton, including with species
595 closely related to *Braarudosphaera* [25].
596
597 We observed two ASVs of UCYN-A, each an exact match to a 16S rRNA gene
598 sequence from genome sequenced UCYN-A types. One ASV was a perfect match to
599 UCYN-A1 (gi|284809060) and another with a perfect match UCYN-A2
600 (gi|671395793) (Figure 4, Supplementary Figure 7). These two ASVs differed by 3
601 bp over the 375 bp 16S rRNA gene sequences that we analyzed. The dynamics of the
602 rRNA gene relative abundance of the UCYN-A1 and UCYN-A2 were similar over the
603 full time-series (Spearman r= 0.64). There was a pronounced increase in both types
604 from 18 April to 25 April when UCYN-A1 increased from about 0.5% to about 3% in
605 rRNA gene proportions of all phytoplankton, while the increase in UCYN-A2 was less
606 pronounced (it peaked to about 1.5% on 25 April). Both UCYN-A types also peaked
607 in early March -- though the peaks were offset slightly (by one day via rRNA gene
608 sequences, two days via rRNA sequences). Both were relatively low in early and late
609 April. Overall, the rRNA levels of the two UCYN-A ASVs were similar in dynamics to
610 the rRNA gene and to one another (Figure 4), though the mid-to-late April peaks
611 were more similar in amplitude and timing in the rRNA than the rRNA gene when
612 UCYN-A1 was about twice as relatively abundant.
613
614 A single *Braarudosphaera bigelowii* ASV (1 bp different over 368 bp to an NCBI 16S
615 rRNA chloroplast gene sequence from *Braarudosphaera, Accession:* AB847986.2
616 [64]) was high in rRNA read proportions during March, low in early April, peaked
617 during the middle of April and decreased after April 24 (Figure 4). The rRNA and
618 rRNA gene of *Braarudosphaera* chloroplasts were correlated (0.64, $p < 0.001$).
619

620 In general, *Braarudosphaera* and UCYN-A were highly positively correlated, and the
621 best correlations were between the *Braarudosphaera rRNA gene* and UCYN-A1 rRNA
622 gene (r= 0.86, Figure 4c), while the correlation to UCYN-A2 rRNA genes was not as
623 strong (r = 0.76) (Supplementary Table 2). *Braarudosphaera* rRNA was correlated to
624 both UCYN-A1 and UCYN-A2 rRNA (r=0.81 and 0.83, respectively). UCYN-A1 rRNA
625 gene was also significantly correlated to *Braarudosphaera* rRNA (r = 0.63), but the
626 other combinations of rRNA to rRNA gene and vice-versa between these two taxa
627 were not as significantly correlated (i.e., $p > 0.005$). Given that the literature reports
628 a specific relationship between UCYN-A2 and *Braarudosphaera* and between UCYN-
629 A1 and a *Haptophyta* taxon closely related to *Braarudosphaera* [25], it may be that
630 the 16S rRNA gene sequence does not discriminate between distinct
631 *Braarudosphaera* or other taxa of *Haptophyta* that may be present.
632
633 We found that there were several other ASVs highly correlated to *Braarudosphaera,*
634 suggesting, at least, shared ecological preferences between these taxa and
635 *Braarudosphaera.* A dictyochophyte alga (*Dictyochophyraceae*_ sp._6) (rRNA) had a
636 particularly strong correlation to *Braarudosphaera* rRNA (r = 0.86). Additionally,
637 *Puniceicoccaceae*_1 and *Puniceicoccaceae*_2 (*Verrucomicrobia*) rRNA and rRNA gene
638 were both very strongly correlated to *Braarudosphaera* (all r >0.81).
639 *Puniceicoccaceae*_2 was strongly correlated to UCYN-A1_1. Generally,
640 *Verrucomicrobia* are often found to be particle associated [7,65–67], and were
641 indeed enriched in the larger size fraction in our samples, suggesting possible
642 physical attachment in an association. FISH targeting *Braarudosphaera*, the two
643 UCYN-A ASVs, and the other potentially associated taxa could be used to
644 substantiate the correlative-based associations we report here.
645
646 *Mesodinium and Teleaulax*
647 Another known interaction between abundant taxa we observed is that of the ciliate
648 *Mesodinium rubrum (=Myrionecta rubra)* with the photosynthetic cryptophyte,
649 *Teleaulax.* In this interaction, *Mesodinium* phagocytizes *Teleaulax* and retains
650 functioning *Telaulax* chloroplast within the *Mesodinium* cell, becoming functionally

651 phototrophic [68]. The exact nature and mechanisms of the interaction is unclear,
652 but the *Teleaulax* chloroplasts can remain intact and apparently funtional for days to
653 weeks within the *Mesodinium* [69,70]. It is unclear to what extent the relationship is
654 most similar to kleptochloroplastic relationships, whereby chloroplasts are
655 consumed and used until they lose function without nuclear assistance; or a
656 karyokleptic relationship, whereby chloroplasts can be maintained by consuming
657 and retention of the nucleus of grazed *Teleaulax* [69]. Further, a dinoflagellate,
658 *Dinophysis,* obtains its chloroplasts by feeding on *Mesodinium*, which in that case
659 would be an intermediate source from *Telaulax* [71,72].
660
661 We found that *Mesodinium* and *Teleaulax* sequences were generally among the
662 highest taxa in overall rRNA gene sequence proportions found in the eukaryotic
663 community (18S rRNA gene) and phytoplankton communities (via 16S rRNA gene
664 sequences of chloroplasts), respectively (Figure 3, Supplementary 4 and 7). On
665 average, the *Teleaulax* ASV (an exact sequence match over the full 374 bp to
666 *Teleaulax amphioxeia,* Supplementary Figure 9) made up 5.5% and 12.4% of
667 chloroplast rRNA gene and rRNA, respectively. The most abundant *Mesodinium* OTU
668 (an exact match to *Mesodinium major* strain LGC-2011, Supplementary Figure 10)
669 made up 2.0% and 2.5% of 18S rRNA gene and rRNA sequences (Figure 5),
670 respectively. The rRNA gene sequences of these taxa increased in abundance
671 between 15 April and 20 April, and again between 24 April and 26 April. The
672 Spearman correlation between the rRNA gene of these taxa (*Mesodinium* and
673 *Teleaulax_amphioxea_1* chloroplasts) was 0.86 and neither taxa had significant
674 correlations to any other taxa (Figure 5d).
675
676 A second abundant *Teleaulax* chloroplast sequence (3 bp different from the best
677 match, *Teleaulax amphioxeia*) was also commonly detected with an average
678 sequence proportion of 2.0% and 1.6% of rRNA gene and rRNA sequences,
679 respectively. This *Teleaulax* chloroplast ASV was not significantly correlated with
680 *Mesodinium.* However, it was significantly correlated with a *Teleaulax* 18S rRNA
681 gene OTU ($r = 0.67$, $p < 0.005$, Figure 5d). Unlike the *Mesodinium-Teleaulax*

682 association, these *Teleaulax* sequences were positively correlated with many ASVs,
683 rRNA genes of *Synechococcus*, *Alphaproteobacteria* (OCS116 and *Defluuivicoccus*),
684 the NS5 genus of *Bacteroidetes*, Marine Group II *Euryarchaeota*, and *Sphingobacteria*
685 (all $r > 0.7$). Finally, while we observed *Dinophysis* in our samples (Supplementary
686 Figure 4-5), they did not have significant correlations to support a *Mesodinium* or
687 *Teleaulax* interaction; however such a statistical relationship may not be expected if
688 the abundance of *Dinophysis* is not dependent on contemporaneous availability of
689 *Mesodinium-Teleaulax* via a specific grazing dependency.
690
691 Our observations of strong, consistent relationship over about 1.5 months between
692 specific types of *Mesodinium* and chloroplasts from *Teleaulax* lends support to the
693 hypothesis that that *Mesodinium* can maintain chloroplasts a long time with the
694 periodic help of *Teleaulax* nuclei [69]. Additionally, based on correlation between
695 *Teleaulax* 18S rRNA gene OTU and a second *Teleaulax* 16S rRNA gene ASV, it
696 appears a second strain of free-living *Teleaulax* is present that may not be
697 associated with *Mesodinium* cells. Because a single *Teleaulax* nucleus in a
698 *Mesodinium* cell might support replication of many more captured chloroplasts than
699 would be found in a single *Teleaulax* cell [69], detection of associated *Teleaulax*
700 nuclei might be hard to discern via correlations between 18S rRNA genes in our
701 system. Other *Teleaulax* nuclei may be present but in lesser abundance (and 18S
702 rRNA gene copies per cell), reducing the ability to regularly detect them in strong
703 co-occurrence with the *Teleaulax* chloroplasts and *Mesodinium*.
704
705 *Other correlations between taxa*
706 To gain an understanding for how the communities changed in relation to one
707 another, overall, we performed Mantel tests. All the different communities were
708 significantly correlated ($p < 0.001$). The non-phytoplankton (regardless of which
709 non-phytoplankton dataset is considered) were more strongly related to the
710 phytoplankton rRNA gene dataset than phytoplankton rRNA dataset
711 (Supplementary Figure 11). The strong correlation between phytoplankton and
712 non-phytoplankton is similar to those that we previously reported [7]. The types of

713 interactions that are driving this strong correlation is unclear, but could be
714 symbiotic, mutualistic, or antagonistic [1,2,73,74]. Another hypothesis is that
715 different phytoplankton communities generate different suspended and sinking
716 marine aggregates that in turn harbor different bacterial and archaeal communities.
717 Further substantiation and insight into these associations will require a variety of
718 techniques, including microscopy, single cell isolation, and ultimately cultivation.
719 There was a relatively weak correlation between *Eukaryota* by 18S rRNA and rRNA
720 gene sequences to the other communities, as has also been shown in another time-
721 series study [75]. This may be because phagotrophs are less species-specific (e.g.,
722 phagocytize all similarly sized taxa) [76,77].
723
724 For pairwise correlations, several of the phytoplankton-to-heterotrophic bacteria
725 correlations are the same as those that we previously reported [7], including those
726 between *Rhodobacteraceae*, *Polaribacter* (*Flavobacteriaceae*), and SAR92 to diatoms
727 *Pseudo-nitzschia* and *Chaetoceros* (Figure 6), suggesting that these correlations are
728 specific and repeatable between different time-series even though they were
729 separated by 3 years and about 20 km. The associations of these prokaryotic groups
730 with phytoplankton, especially in diatom blooms, have been reported previously,
731 with responses at time-scales from weeks to months [6,9,11,60]. We also observed a
732 group of highly positively correlated *Prochlorococcus* ASV to various taxa from
733 *Flavobacteriaceae* and *Verrucomicrobia*, indicating the shared ecosystem
734 preferences or interactions (Figure 6).
735
736 In addition to the types of interactions previously described, we also observed many
737 strong correlations between heterotrophic or mixotrophic eukaryotic taxa and
738 potential symbionts or prey (Figure 7). Of these, only five taxa had strong
739 correlations (|Spearman r | > 0.7, $p < 0.005$) to bacteria or phytoplankton; of these,
740 four were ciliates. In addition to the relationship between *Mesodinium* and *Teleaulax*
741 described previously, the ciliate OTUs of *Strombidium* were shown to have
742 correlations to a variety of *Bacteria*, including *Flavobacteriaceae*,
743 *Gammaproteobacteria*, relatively rare ASVs classified as *Mycoplasma*, and *Pseudo-*

744 *nitzschia*. We observed no strong negative correlations (Spearman $r < -0.7$), in
745 contrast to many strong positive ones > 0.7 or even 0.8. Even though these taxa are
746 positively associated (seemingly implying mutual benefice), it is unclear if predator-
747 prey interactions would be expected to be positively or negatively correlated on this
748 time-scale. This would likely depend on factors such as specificity and turnover
749 times of the taxa involved. However, it appears that these particular ciliates may
750 have specific interactions with these bacteria, and may be good targets for future
751 analyses to determine the nature of these interactions.
752
753 **Conclusions**
754 Our results show a rapid, day-to-day response of particular microbial taxa to
755 changes in phytoplankton. In our study, we saw only a small increase in
756 phytoplankton biomass, relative to previous studies, yet many of the patterns
757 previously observed persisted. Observations of microbial dynamics via rRNA and
758 rRNA gene yielded somewhat similar results, though the overall proportions of taxa
759 could change between the rRNA and rRNA gene sequence datasets, with
760 phytoplankton often being the more represented among rRNA sequences. Our
761 results provide new *in-situ* characterizations of previously reported symbiotic
762 interactions which were between taxa with some of the highest average sequence
763 proportions that we observed across the whole time-series. These observations
764 suggested that the *Mesodinium*-to-*Teleaulax* chloroplast association appeared to
765 occur independently of other microbial interactions, while UCYN-A-to-
766 *Braarudosphaera* co-occurred with several other taxa. Overall, the study reiterates
767 the utility of short-term time-series for understanding environmental responses and
768 microbe-to-microbe interactions in which turnover times can be very fast.
769
770
771
772
773
774

Acknowledgements

We thank the Gordon and Betty Moore Foundation for funding (Grant Number: 3779) and their support of this project. We thank the Scholin Lab at the Monterey Bay Aquarium Research Institute for deployment, data acquisition, quality control, and help with experimental design. In particular we thank Christina Preston, Roman Marin III, James Birch, Scott Jensen, Brent Roman, Bill Ussler, and Kevan Yamahara for their help with the ESP, and Charlotte Eckmann for valuable comments on the manuscript. We thank the Wrigley Institute of Environmental Studies for logical support, especially Gordon Boivin. We thank the National Science Foundation for financial support (Grant Number: 1136818).

Conflicts of Interest

The authors declare no conflict of interest

References

1. Worden AZ, Follows MJ, Giovannoni SJ, Wilken S, Zimmerman AE, Keeling PJ. Rethinking the marine carbon cycle: Factoring in the multifarious lifestyles of microbes. Science. 2015;347:1257594–1257594.

2. Fuhrman JA, Cram JA, Needham DM. Marine microbial community dynamics and their ecological interpretation. Nat Rev Microbiol. 2015;13:133–46.

3. Gilbert JA, Steele JA, Caporaso JG, Steinbrück L, Reeder J, Temperton B, et al. Defining seasonal marine microbial community dynamics. ISME J. 2012;6:298–308.

4. Fuhrman JA, Hewson I, Schwalbach MS, Steele JA, Brown M V., Naeem S. Annually reoccurring bacterial communities are predictable from ocean conditions. Proc Natl Acad Sci U S A. 2006;103:13104–9.

5. Cram JA, Chow C-ET, Sachdeva R, Needham DM, Parada AE, Steele JA, et al. Seasonal and interannual variability of the marine bacterioplankton community throughout the water column over ten years. ISME J. 2014;9:563.

6. Teeling H, Fuchs BM, Becher D, Klockow C, Gardebrecht A, Bennke CM, et al. Substrate-controlled succession of marine bacterioplankton populations induced by a phytoplankton bloom. Science. 2012;336:608–11.

806 7. Needham DM, Fuhrman JA. Pronounced daily succession of phytoplankton,
807 archaea and bacteria following a spring bloom. Nat Microbiol. 2016;1:16005.
808 8. Fuhrman JA, Azam F. Thymidine incorporation as a measure of heterotrophic
809 bacterioplankton production in marine surface waters: Evaluation and field results.
810 Mar Biol. 1982;66:109–20.
811 9. Teeling H, Fuchs BM, Bennke CM, Krüger K, Chafee M, Kappelmann L, et al.
812 Recurring patterns in bacterioplankton dynamics during coastal spring algae
813 blooms. Elife. 2016;5:1–31.
814 10. Needham DM, Sachdeva R, Fuhrman JA. Ecological dynamics and co-occurrence
815 among marine phytoplankton, bacteria and myoviruses shows microdiversity
816 matters. ISME J. 2017;11:1614–29.
817 11. Buchan A, LeCleir GR, Gulvik CA, González JM. Master recyclers: features and
818 functions of bacteria associated with phytoplankton blooms. Nat Rev Microbiol.
819 2014;12:686–98.
820 12. Mitra A, Flynn KJ, Tillmann U, Raven JA, Caron DA, Stoecker DK, et al. Defining
821 planktonic protist functional groups on mechanisms for energy and nutrient
822 acquisition: incorporation of diverse mixotrophic strategies. Protist. Elsevier GmbH.;
823 2016;167:106–20.
824 13. Graf JS, Thingstad TF. The ecological role of water-column microbes in the sea.
825 Mar Ecol. 1983;10:257–63.
826 14. Parada AE, Needham DM, Fuhrman JA. Every base matters: assessing small
827 subunit rRNA primers for marine microbiomes with mock communities, time-series
828 and global field samples. Environ Microbiol. 2016;18:1403–14.
829 15. Eren AM, Morrison HG, Lescault PJ, Reveillaud J, Vineis JH, Sogin ML. Minimum
830 entropy decomposition: Unsupervised oligotyping for sensitive partitioning of high-
831 throughput marker gene sequences. ISME J. 2014;9:968–79.
832 16. Callahan BJ, Mcmurdie PJ, Rosen MJ, Han AW, Johnson AJ, Holmes SP. DADA2 :
833 High resolution sample inference from amplicon data. Nat Methods. 2016;13:581–3.
834 17. Tikhonov M, Leach RW, Wingreen NS. Interpreting 16S metagenomic data
835 without clustering to achieve sub-OTU resolution. ISME J. Nature Publishing Group;
836 2015;9:68–80.

837 18. Campbell BJ, Yu L, Heidelberg JF, Kirchman DL. Activity of abundant and rare
838 bacteria in a coastal ocean. Proc Natl Acad Sci U S A. 2011;108:12776–81.
839 19. Hunt DE, Lin Y, Church MJ, Karl DM, Tringe SG, Izzo LK, et al. Relationship
840 between abundance and specific activity of bacterioplankton in open ocean surface
841 waters. Appl Environ Microbiol. 2013;79:177–84.
842 20. Blazewicz SJ, Barnard RL, Daly RA, Firestone MK. Evaluating rRNA as an
843 indicator of microbial activity in environmental communities: limitations and uses.
844 ISME J. Nature Publishing Group; 2013;7:2061–8.
845 21. Lankiewicz TS, Cottrell MT, Kirchman DL. Growth rates and rRNA content of four
846 marine bacteria in pure cultures and in the Delaware estuary. ISME J. Nature
847 Publishing Group; 2016;10:823–32.
848 22. Brown M V., Fuhrman JA. Marine bacterial microdiversity as revealed by internal
849 transcribed spacer analysis. Aquat Microb Ecol. 2005;41:15–23.
850 23. de Vargas C, Audic S, Henry N, Decelle J, Mahé F, Logares R, et al. Eukaryotic
851 plankton diversity in the sunlit ocean. Science. 2015;348:1261605-1–11.
852 24. Johnson MD, Beaudoin DJ, Laza-Martinez A, Dyhrman ST, Fensin E, Lin S, et al.
853 The genetic diversity of *Mesodinium* and associated cryptophytes. Front Microbiol.
854 2016. p. 2017.
855 25. Zehr JP, Shilova IN, Farnelid HM, Muñoz-Marín M del C, Turk-Kubo KA. Unusual
856 marine unicellular symbiosis with the nitrogen-fixing cyanobacterium UCYN-A. Nat
857 Microbiol. 2016;2:1:10.
858 26. Scholin C, Doucette G, Jensen S, Roman B, Pargett D, Marin RI, et al. Remote
859 detection of marine microbes, small invertebrates, harmful algae, and biotoxins
860 using the Environmental Sample Processor (ESP). Oceanography. 2009;22:158–67.
861 27. Ottesen EA, Marin R, Preston CM, Young CR, Ryan JP, Scholin CA, et al.
862 Metatranscriptomic analysis of autonomously collected and preserved marine
863 bacterioplankton. ISME J. 2011;5:1881–95.
864 28. Gray MA, Pratte ZA, Kellogg CA. Comparison of DNA preservation methods for
865 environmental bacterial community samples. FEMS Microbiol Ecol. 2013;83:468–
866 77.
867 29. McCarthy A, Chiang E, Schmidt ML, Denef VJ. RNA preservation agents and

868 nucleic acid extraction method bias perceived bacterial community composition.
869 PLoS One. 2015;10:1–14.
870 30. Trinh RC, Fichot CG, Gierach MM, Holt B, Malakar NK, Hulley G, et al. Application
871 of Landsat 8 for monitoring impacts of wastewater discharge on coastal water
872 quality. Front Mar Sci. 2017;4:329.
873 31. Fuhrman JA, Comeau DE, Hagstrom A, Chan AM. Extraction from natural
874 planktonic microorganisms of DNA suitable for molecular biological studies. Appl
875 Environ Microbiol. 1988;54:1426–9.
876 32. Countway PD, Gast RJ, Savai P, Caron DA. Protistan diversity estimates based on
877 18S rDNA from seawater incubations in the western North Atlantic. J Eukaryot
878 Microbiol. 2005;52:95–106.
879 33. Edgar RC. UPARSE: highly accurate OTU sequences from microbial amplicon
880 reads. Nat Methods. 2013;10:996–8.
881 34. Martin M. Cutadapt removes adapter sequences from high-throughput
882 sequencing reads. EMBnet.journal. 2011;17.
883 35. Pruesse E, Quast C, Knittel K, Fuchs BM, Ludwig W, Peplies J, et al. SILVA: a
884 comprehensive online resource for quality checked and aligned ribosomal RNA
885 sequence data compatible with ARB. Nucleic Acids Res. 2007;35:7188–96.
886 36. Caporaso JG, Kuczynski J, Stombaugh J, Bittinger K, Bushman FD, Costello EK, et
887 al. QIIME allows analysis of high-throughput community sequencing data. Nat
888 Methods. 2010;7:335–6.
889 37. Eren AM, Maignien L, Sul WJ, Murphy LG, Grim SL, Morrison HG, et al.
890 Oligotyping: Differentiating between closely related microbial taxa using 16S rRNA
891 gene data. Methods Ecol Evol. 2013;4:1111–9.
892 38. McDonald D, Price MN, Goodrich J, Nawrocki EP, DeSantis TZ, Probst A, et al. An
893 improved Greengenes taxonomy with explicit ranks for ecological and evolutionary
894 analyses of bacteria and archaea. ISME J. Nature Publishing Group; 2012;6:610–8.
895 39. Decelle J, Romac S, Stern RF, Bendif EM, Zingone A, Audic S, et al. PhytoREF: a
896 reference database of the plastidial 16S rRNA gene of photosynthetic eukaryotes
897 with curated taxonomy. Mol Ecol Resour. 2015;15:1435–45.
898 40. Edgar RC. Search and clustering orders of magnitude faster than BLAST.

899 Bioinformatics. 2010;26:2460–1.
900 41. Altschul SF, Gish W, Miller W, Myers EW, Lipman DJ. Basic local alignment search
901 tool. J Mol Biol. 1990;215:403–10.
902 42. Zehr JP, Bench SR, Carter BJ, Hewson I, Niazi F, Shi T, et al. Globally distributed
903 uncultivated oceanic N2-fixing cyanobacteria lack oxygenic photosystem II. Nature.
904 2008;322:1110–2.
905 43. Bombar D, Heller P, Sanchez-Baracaldo P, Carter BJ, Zehr JP. Comparative
906 genomics reveals surprising divergence of two closely related strains of
907 uncultivated UCYN-A cyanobacteria. ISME J. Nature Publishing Group; 2014;8:2530–
908 42.
909 44. Zhang J, Kobert K, Flouri T, Stamatakis A. PEAR: a fast and accurate Illumina
910 Paired-End reAd mergeR. Bioinformatics. Oxford University Press; 2014;30:614–20.
911 45. Jeraldo P, Kalari K, Chen X, Bhavsar J, Mangalam A, White B, et al. IM-TORNADO:
912 a tool for comparison of 16S reads from paired-end libraries. PLoS One.
913 2014;9:e114804.
914 46. Wang Q, Garrity GM, Tiedje JM, Cole JR. Naïve Bayesian classifier for rapid
915 assignment of rRNA sequences into the new bacterial taxonomy. Appl Environ
916 Microbiol. American Society for Microbiology; 2007;73:5261–7.
917 47. Edgar RC. MUSCLE: Multiple sequence alignment with high accuracy and high
918 throughput. Nucleic Acids Res. 2004;32:1792–7.
919 48. Guindon S, Dufayard J, Lefort V, Anisimova M, Hordijk W, Gascuel O. New
920 algorithms and methods to estimate maximum-likelihood phylogenies: Assessing
921 the performance of PhyML 3.0. Syst Biol. 2010;59:307–21.
922 49. Johnson MD, Tengs T, Oldach DW, Delwiche CF, Stoecker DK. Highly divergent
923 SSU rRNA genes found in the marine ciliates *Myrionecta rubra* and *Mesodinium*
924 *pulex*. Protist. 2004;155:347–59.
925 50. Xia LC, Steele JA, Cram JA, Cardon ZG, Simmons SL, Vallino JJ, et al. Extended local
926 similarity analysis (eLSA) of microbial community and other time series data with
927 replicates. BMC Syst Biol. BioMed Central Ltd; 2011;5:1–12.
928 51. Xia LC, Ai D, Cram JA, Fuhrman JA, Sun F. Efficient statistical significance
929 approximation for local similarity analysis of high-throughput time series data.

930 Bioinformatics. 2013;29:230–7.
931 52. R Core Team. R: A Language and Environment for Statistical Computing. Vienna,
932 Austria; 2015.
933 53. Oksanen AJ, Blanchet FG, Kindt R, Legendre P, Minchin PR, Hara RBO, et al.
934 vegan: Community Ecology Package. 2015;
935 54. Dandonneau Y, Neveux J. Diel variations of in vivo fluorescence in the eastern
936 equatorial Pacific: an unvarying pattern. Deep Res Part II Top Stud Oceanogr.
937 1997;44:1869–80.
938 55. Fuhrman JA, Schwalbach MS, Stingl U. Proteorhodopsins: an array of
939 physiological roles? Nat Rev Micro. Nature Publishing Group; 2008;6:488–94.
940 56. Béjà O, Suzuki MT, Heidelberg JF, Nelson WC, Preston CM, Hamada T, et al.
941 Unsuspected diversity among marine aerobic anoxygenic phototrophs. Nature.
942 2002;415:630–3.
943 57. Schwalbach MS, Fuhrman JA. Wide-ranging abundances of aerobic anoxygenic
944 phototrophic bacteria in the world ocean revealed by epifluorescence microscopy
945 and quantitative PCR. Limnol Oceanogr. 2005;50:620–8.
946 58. Könneke M, Bernhard AE, de la Torre JR, Walker CB, Waterbury JB, Stahl DA.
947 Isolation of an autotrophic ammonia-oxidizing marine archaeon. Nature.
948 2005;437:543–6.
949 59. Hamersley M, Turk K, Leinweber A, Gruber N, Zehr JP, Gunderson T, et al.
950 Nitrogen fixation within the water column associated with two hypoxic basins
951 within the Southern California Bight. Aquat Microb Ecol. 2011;63:193–205.
952 60. Chafee M, Fernàndez-Guerra A, Buttigieg PL, Gerdts G, Eren AM, Teeling H, et al.
953 Recurrent patterns of microdiversity in a temperate coastal marine environment.
954 ISME J. 2017;1–16.
955 61. Farnelid H, Turk-Kubo K, Muñoz-Marín M, Zehr JP. New insights into the ecology
956 of the globally significant uncultured nitrogen-fixing symbiont UCYN-A. Aquat
957 Microb Ecol. 2016;77:125–38.
958 62. Thompson AW, Foster RA, Krupke A, Carter BJ, Musat N, Vaulot D, et al.
959 Unicellular cyanobacterium symbiotic with a single-celled eukaryotic alga. Science.
960 2012;337:1546–50.

961 63. Tripp HJ, Bench SR, Turk K a, Foster R a, DeSantis TZ, Niazi F, et al. Metabolic
962 streamlining in an open-ocean nitrogen-fixing cyanobacterium. Nature.
963 2010;464:90–4.
964 64. Hagino K, Onuma R, Kawachi M, Horiguchi T. Discovery of an endosymbiotic
965 nitrogen-fixing cyanobacterium UCYN-A in *Braarudosphaera bigelowii*
966 (Prymnesiophyceae). PLoS One. 2013;8:e81749.
967 65. Crespo BG, Pommier T, Fernández-Gómez B, Pedrós-Alió C. Taxonomic
968 composition of the particle-attached and free-living bacterial assemblages in the
969 Northwest Mediterranean Sea analyzed by pyrosequencing of the 16S rRNA.
970 Microbiologyopen. 2013;2:541–52.
971 66. Rath J, Wu KY, Herndl GJ, DeLong EF. High phylogenetic diversity in a marine
972 snow-associated bacterial assemblage. Aquat Microb Ecol. 1998;14:261–9.
973 67. Mestre M, Borrull E, Sala Mm, Gasol JM. Patterns of bacterial diversity in the
974 marine planktonic particulate matter continuum. ISME J. 2017;1–12.
975 68. Gustafson DE, Stoecker DK, Johnson MD, Van Heukelem WF, Sneider K.
976 Cryptophyte algae are robbed of their organelles by the marine ciliate *Mesodinium*
977 *rubrum*. Nature. 2000;405:1049–52.
978 69. Johnson MD, Oldach D, Delwiche CF, Stoecker DK. Retention of transcriptionally
979 active cryptophyte nuclei by the ciliate *Myrionecta rubra*. Nature. 2007;445:426–8.
980 70. Herfort L, Peterson TD, McCue LA, Crump BC, Prahl FG, Baptista AM, et al.
981 *Myrionecta rubra* population genetic diversity and its cryptophyte chloroplast
982 specificity in recurrent red tides in the Columbia River estuary. Aquat Microb Ecol.
983 2011;62:85–97.
984 71. Garcia-Cuetos L, Moestrup Ø, Hansen PJ, Daugbjerg N. The toxic dinoflagellate
985 *Dinophysis acuminata* harbors permanent chloroplasts of cryptomonad origin, not
986 kleptochloroplasts. Harmful Algae. 2010;9:25–38.
987 72. Sjöqvist CO, Lindholm TJ. Natural co-occurrence of *Dinophysis acuminata*
988 (Dinoflagellata) and *Mesodinium rubrum* (Ciliophora) in thin layers in a coastal inlet.
989 J Eukaryot Microbiol. 2011;58:365–72.
990 73. Amin SA, Parker MS, Armbrust EV. Interactions between diatoms and bacteria.
991 Microbiol Mol Biol Rev. 2012;76:667–84.

992 74. Amin SA, Hmelo LR, van Tol HM, Durham BP, Carlson LT, Heal KR, et al.
993 Interaction and signalling between a cosmopolitan phytoplankton and associated
994 bacteria. Nature. 2015;522:98–101.
995 75. Chow C-ET, Kim DY, Sachdeva R, Caron DA, Fuhrman JA. Top-down controls on
996 bacterial community structure: microbial network analysis of bacteria, T4-like
997 viruses and protists. ISME J. Nature Publishing Group; 2014;8:816–29.
998 76. Hahn MW, Höfle MG. Flagellate predation on a bacterial model community:
999 Interplay of size-selective grazing, specific bacterial cell size, and bacterial
1000 community composition. Appl Environ Microbiol. American Society for
1001 Microbiology; 1999;65:4863–72.
1002 77. Gonzalez JM, Sherr EB, Sherr BF. Size-selective grazing on bacteria by natural
1003 assemblages of estuarine flagellates and ciliates. Appl Environ Microbiol.
1004 1990;56:583–9.
1005
1006
1007
1008
1009
1010
1011
1012
1013
1014
1015
1016
1017
1018
1019
1020
1021
1022

1023 **Figure Legends**

1024 **Figure 1 | Environmental context for the Environmental Sample Processor**
1025 **(ESP) deployment near Santa Catalina Island 18 Mar-1 May 2014.** Sampling did
1026 not occur for about two weeks 23 Mar - 9 Apr due to ESP disconnection. Before the
1027 interruption, the microbial community was collected daily at 10:00, and, after, twice
1028 daily at 10:00 and 22:00. During the interruption, (**a**) satellite chlorophyll-*a*
1029 measurements indicated a small increase in chlorophyll-*a* occurred throughout the
1030 San Pedro Channel, peaking four days before resumption of sampling. (**b**)
1031 Temperature and depth, and (**c**) chlorophyll-*a* CTD ESP concentrations were
1032 measured every five minutes (the thin lines); chlorophyll-*a* data 12 – 15 April is
1033 missing due to poor quality. Satellite chlorophyll-*a* is the mean of 3-x-3 pixels (~ 3-
1034 x-3 km area) covering the region surrounding the ESP; the error bars are the
1035 standard deviation of the nine pixels used in calculation of the mean. Note, in these
1036 waters, the satellite-derived chlorophyll-*a* concentrations are generally
1037 representative of the upper 5 m of the water column, and the ESP was deployed
1038 between 5-20 m, so some variation in absolute concentration is expected. Tide data
1039 are observed water measurements for nearby Los Angeles, CA. Circles represent the
1040 average value during sample collection for microbial community analyses (usually
1041 about 30 minutes). (**b**) and (**c**) Sample collection times are indicated by ticks at the
1042 top of the figures.

1043

1044 **Figure 2 | Dynamics of the overall proportion of sequences observed using a**
1045 **single "universal" primer.** The data was split into three partitions:
1046 "Phytoplankton" (green, chloroplast and cyanobacterial rRNA and rRNA gene
1047 sequences), "Non-Phytoplankton" (black, all remaining bacterial and archaeal 16S
1048 rRNA and rRNA gene sequences), and *Eukaryota* sequences (red, all 18S rRNA and
1049 rRNA gene sequences). Data are shown for the (**a**) 1-300 μm size fraction rRNA gene
1050 sequences, (**b**) 1-300 μm rRNA sequences, (**c**) 0.2-1 μm rRNA gene sequences, and
1051 (**d**) 0.2-1 μm rRNA sequences. Satellite chlorophyll-*a* concentrations and standard
1052 deviations (shown in yellow) are estimated by 3-x-3 pixels surrounding the ESP as
1053 in Figure 1.

1054 **Figure 3 | Daily to semi-daily 16S and 18S rRNA and rRNA gene dynamics of**
1055 **microbial taxa**. Heatmaps include data from (**a**) "non-phytoplankton" *Bacteria* and
1056 *Archaea* via 16S rRNA and rRNA gene sequences, (**b**) "phytoplankton", via 16S rRNA
1057 and rRNA gene sequences of chloroplasts and *Cyanobacteria*, and (**c**) *Eukaryota* taxa
1058 via 18S rRNA and rRNA gene, excluding metazoan sequences. Only ASVs or OTUs
1059 that ever became taxon with the highest proportion of sequences within a given
1060 dataset for at least one sample are shown. The tree shows the phylogenetic
1061 relatedness of the ASV or OTU according to the amplicon-sequenced region. Note
1062 that *Mesodinium* is known to have a very aberrant 18S rRNA gene sequence [49].
1063 For the dates where two samples were taken per day (10:00 AM and 10:00 PM, 10
1064 April - 1 May), a dash underneath a given sample indicates the sample was taken at
1065 night. All 16S rRNA and rRNA gene ASVs shown here were also detected during the
1066 2011 diatom bloom study [7,10], except where "--" is found next to the ASV name;
1067 asterisks next to taxon names indicate that ASV was also found to most abundant
1068 during the 2011 study.
1069
1070 **Figure 4 | Co-occurrence of symbionts UCYN-A and *Braarudosphaera.*** Relative
1071 proportions are via 16S (**a**) rRNA genes and (**b**) rRNA as proportion of all
1072 phytoplankton chloroplasts and *Cyanobacteria* sequences in the 1-300 μm size
1073 fraction. (**c**) Co-occurrence network of taxa positively correlated to UCYN-A or
1074 *Braarudosphaera* taxa where circles, squares, and diamonds represent
1075 phytoplankton, non-phytoplankton, and *Eukaryota* rRNA and rRNA gene ASVs or
1076 OTUs, respectively. Nodes filled in with gray shading are from the 1-300 μm size
1077 fraction, and those with no shading (open) are from the 0.2-1 μm size fractions,
1078 respectively. Darker gray nodes indicate the UCYN-A and *Braarudosphaera* nodes. A
1079 dashed line surrounding a node indicates the node represents data from the rRNA
1080 dataset, whereas a solid line or no-line indicates rRNA gene. Lines connecting edges
1081 indicate positive correlations (Spearman $r > 0.80$, p & $q < 0.001$) and line thickness
1082 corresponds with strength of correlation.
1083

1084 **Figure 5 | Co-occurrence of symbionts of *Mesodinium rubrum* and *Teleaulax*.**
1085 Dynamics of the dominant ASVs of *Mesodinium* and *Teleaulax* chloroplast via (**a**)
1086 rRNA gene sequences, and (**b**) rRNA sequences. Additionally, the dynamics of a (**c**)
1087 second *Teleaulax* chloroplast ASV and the *Teleaulax* with highest sequence
1088 proportions via 18S rRNA genes. (**d**) Co-occurrence network of taxa positively
1089 correlated to *Mesodinium* and *Teleaulax* showing that the dynamics of the apparent
1090 symbionts are not correlated to other taxa. Network colors and shapes are the same
1091 as in Figure 4.
1092
1093 **Figure 6 | Network showing pairwise positive correlations between**
1094 **phytoplankton and non-phytoplankton or *Eukaryota* rRNA and rRNA ASV or**
1095 **OTU relative proportions.** As in Figure 4, nodes filled in with gray shading are
1096 from the 1-300 μm size fraction and those with no shading (open) are from the 0.2-1
1097 μm size fraction. A dashed line surrounding a node indicates the node represents
1098 data from the rRNA sequence dataset, whereas a solid line or no-line indicates rRNA
1099 gene sequence dataset. Connecting lines indicate positive correlations (Spearman >
1100 0.80, p & q < 0.001) and line thickness corresponds with strength of correlation.
1101 Only taxa with average relative abundance > 0.5% are shown.
1102
1103 **Figure 7 | Network showing pairwise positive correlations between**
1104 **heterotrophic *Eukaryota* to *Bacteria* and phytoplankton.** Vertical lines
1105 surrounding a node indicates the node represents data from the rRNA sequence
1106 dataset, whereas no-line indicates rRNA gene sequence dataset. Lines connecting
1107 edges indicate correlations (Spearman > 0.70, p & q < 0.001; no correlations were
1108 observed < -0.70) and line thickness corresponds with strength of correlation. MAST
1109 heterotrophs would not show (see methods).
1110

Figure 1

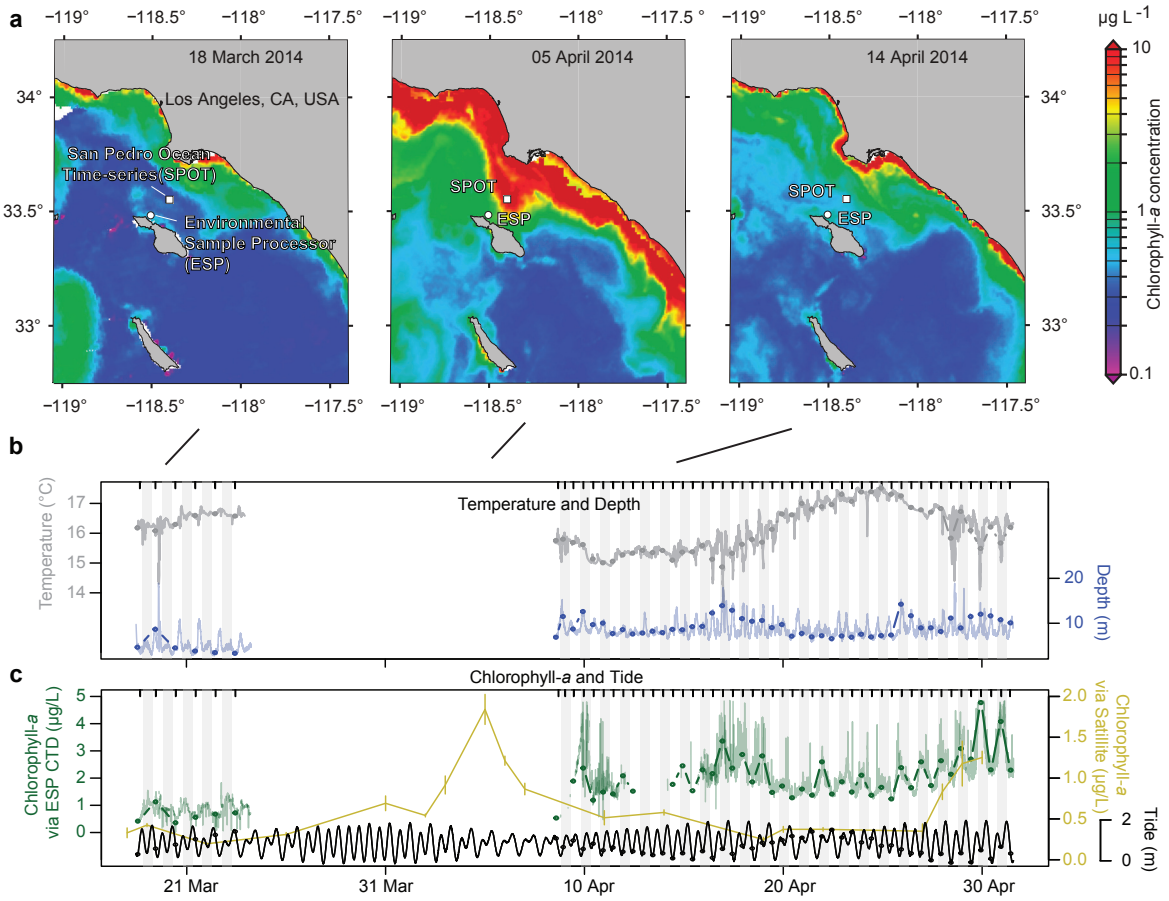

Figure 1 | Environmental context for the Environmental Sample Processor (ESP) deployment near Santa Catalina Island 18 Mar-1 May 2014. Sampling did not occur for about two weeks 23 Mar - 9 Apr due to ESP disconnection. Before the interruption, the microbial community was collected daily at 10:00, and, after, twice daily at 10:00 and 22:00. During the interruption, (**a**) satellite chlorophyll-*a* measurements indicated a small increase in chlorophyll-a occurred throughout the San Pedro Channel, peaking four days before resumption of sampling. (**b**) Temperature and depth, and (**c**) chlorophyll-*a* CTD ESP concentrations were measured every five minutes (the thin lines); chlorophyll-a data 12 – 15 April is missing due to poor quality. Satellite chlorophyll-a is the mean of 3-x-3 pixels (~ 3-x-3 km area) covering the region surrounding the ESP; the error bars are the standard deviation of the nine pixels used in calculation of the mean. Note, in these waters, the satellite-derived chlorophyll-a concentrations are generally representative of the upper 5 m of the water column, and the ESP was deployed between 5-20 m, so some variation in absolute concentration is expected. Tide data are observed water measurements for nearby Los Angeles, CA. Circles represent the average value during sample collection for microbial community analyses (usually about 30 minutes). (**b**) and (**c**) Sample collection times are indicated by ticks at the top of the figures.

Figure 2

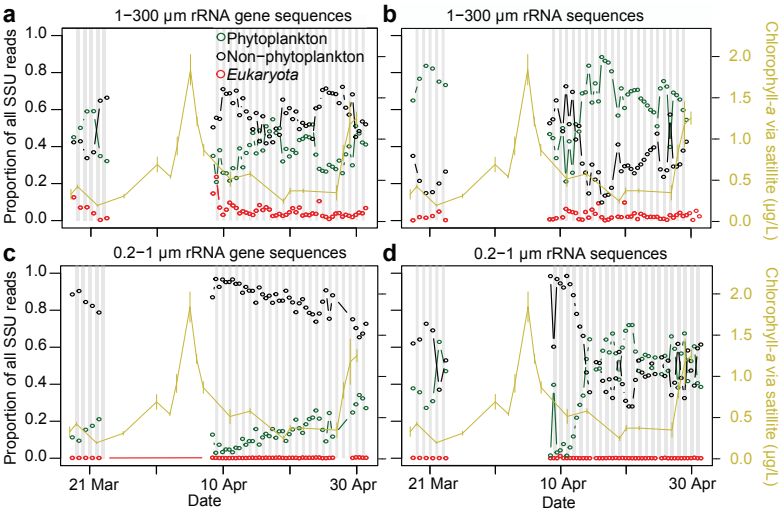

Figure 2 | Dynamics of the overall proportion of sequences observed using a single "universal" primer. The data was split into three partitions: "Phytoplankton" (green, chloroplast and cyanobacterial rRNA and rRNA gene sequences), "Non-Phytoplankton" (black, all remaining bacterial and archaeal 16S rRNA and rRNA gene sequences), and *Eukaryota* sequences (red, all 18S rRNA and rRNA gene sequences). Data are shown for the (**a**) 1-300 µm size fraction rRNA gene sequences, (**b**) 1-300 µm rRNA sequences, (**c**) 0.2-1 µm rRNA gene sequences, and (**d**) 0.2-1 µm rRNA sequences. Satellite chlorophyll-*a* concentrations and standard deviations (shown in yellow) are estimated by 3-x-3 pixels surrounding the ESP as in Figure 1.

Figure 3

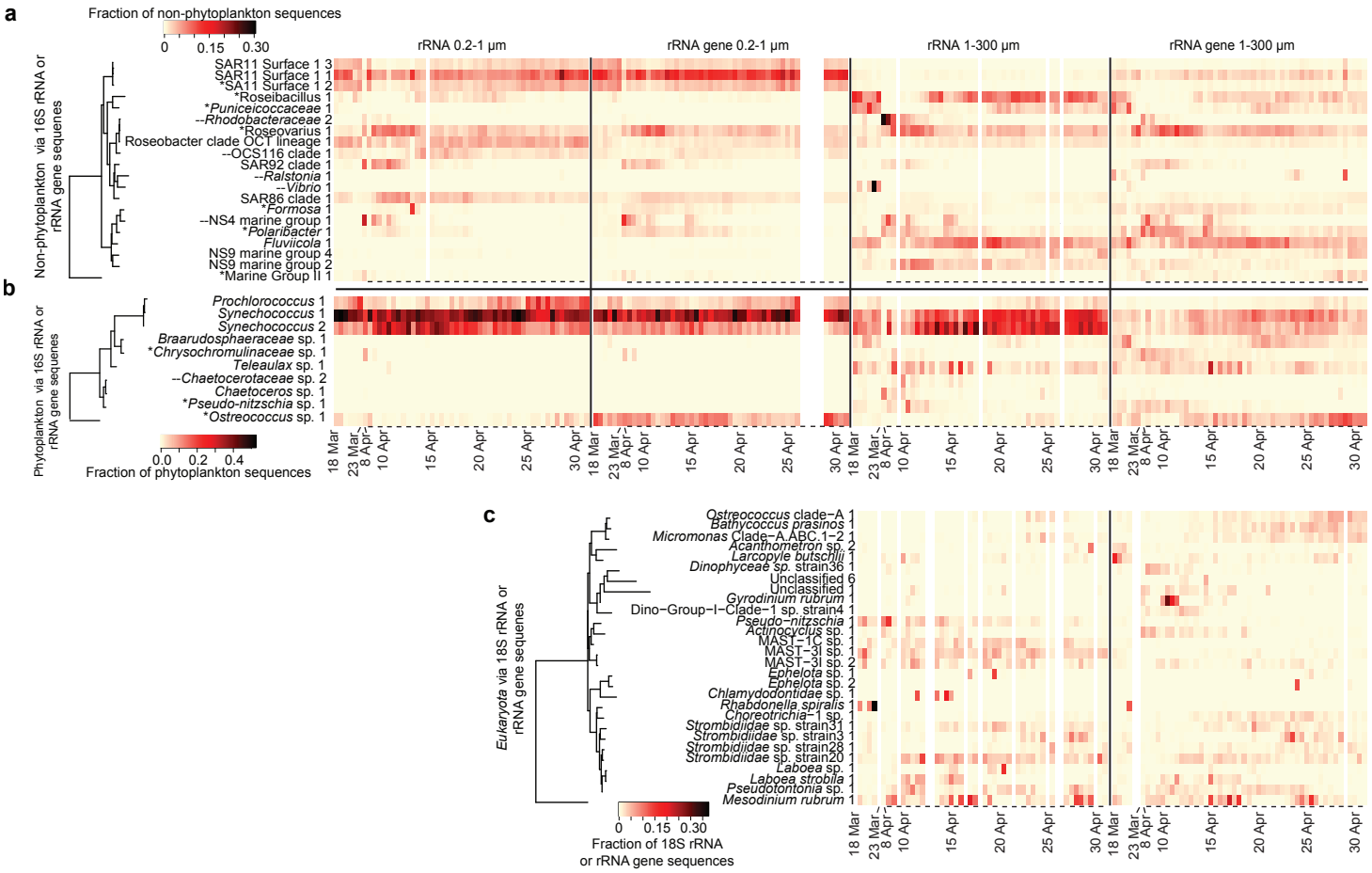

Figure 3 | Daily to semi-daily 16S and 18S rRNA and rRNA gene dynamics of microbial taxa. Heatmaps include data from (**a**) "non-phytoplankton" Bacteria and Archaea via 16S rRNA and rRNA gene sequences, (**b**) "phytoplankton", via 16S rRNA and rRNA gene sequences of chloroplasts and Cyanobacteria, and (**c**) *Eukaryota* taxa via 18S rRNA and rRNA gene, excluding metazoan sequences. Only ASVs or OTUs that ever became taxon with the highest proportion of sequences within a given dataset for at least one sample are shown. The tree shows the phylogenetic relatedness of the ASV or OTU according to the amplicon-sequenced region. Note that Mesodinium is known to have a very aberrant 18S rRNA gene sequence [49]. For the dates where two samples were taken per day (10:00 AM and 10:00 PM, 10 April - 1 May), a dash underneath a given sample indicates the sample was taken at night. All 16S rRNA and rRNA gene ASVs shown here were also detected during the 2011 diatom bloom study [7,10], except where "--" is found next to the ASV name; asterisks next to taxon names indicate that ASV was also found to most abundant during the 2011 study.

Figure 4

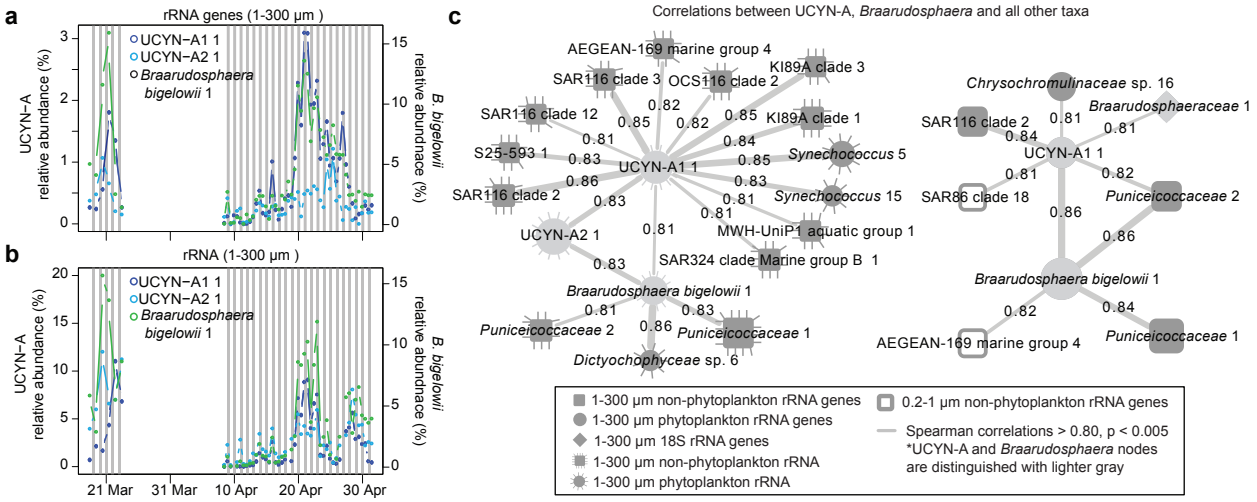

Figure 4 | Co-occurrence of symbionts UCYN-A and Braarudosphaera. Relative proportions are via 16S (**a**) rRNA genes and (**b**) rRNA as proportion of all phytoplankton chloroplasts and Cyanobacteria sequences in the 1-300 µm size fraction. (**c**) Co-occurrence network of taxa positively correlated to UCYN-A or *Braarudosphaera* taxa where circles, squares, and diamonds represent phytoplankton, non-phytoplankton, and Eukaryota rRNA and rRNA gene ASVs or OTUs, respectively. Nodes filled in with gray shading are from the 1-300 µm size fraction, and those with no shading (open) are from the 0.2-1 µm size fractions, respectively. Darker gray nodes indicate the UCYN-A and *Braarudosphaera* nodes. A dashed line surrounding a node indicates the node represents data from the rRNA dataset, whereas a solid line or no-line indicates rRNA gene. Lines connecting edges indicate positive correlations (Spearman $r > 0.80$, p & $q < 0.001$) and line thickness corresponds with strength of correlation.

Figure 5

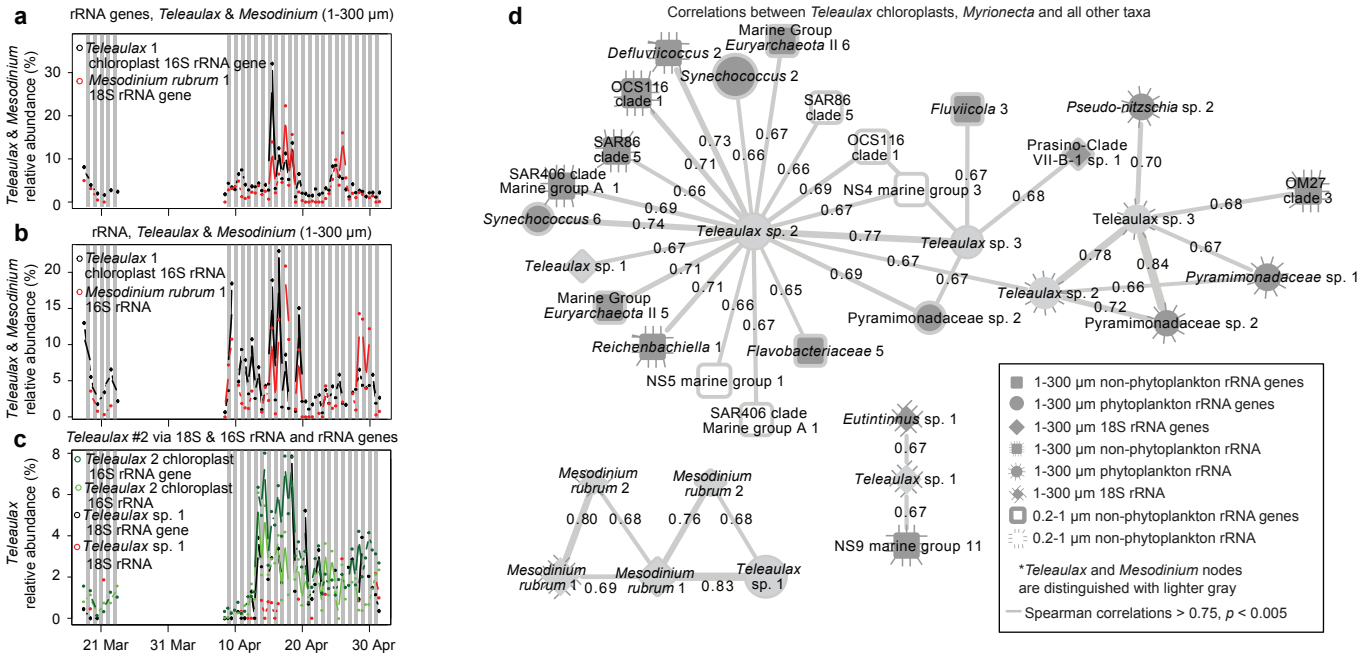

Figure 5 | Co-occurrence of symbionts of *Mesodinium rubrum* and *Teleaulax*. Dynamics of the dominant ASVs of *Mesodinium* and *Teleaulax* chloroplast via (**a**) rRNA gene sequences, and (**b**) rRNA sequences. Additionally, the dynamics of a (c) second Teleaulax chloroplast ASV and the Teleaulax with highest sequence proportions via 18S rRNA genes. (d) Co-occurrence network of taxa positively correlated to *Mesodinium* and *Teleaulax* showing that the dynamics of the apparent symbionts are not correlated to other taxa. Network colors and shapes are the same as in Figure 4.

Figure 6

Correlations between phytoplankton and all other taxa

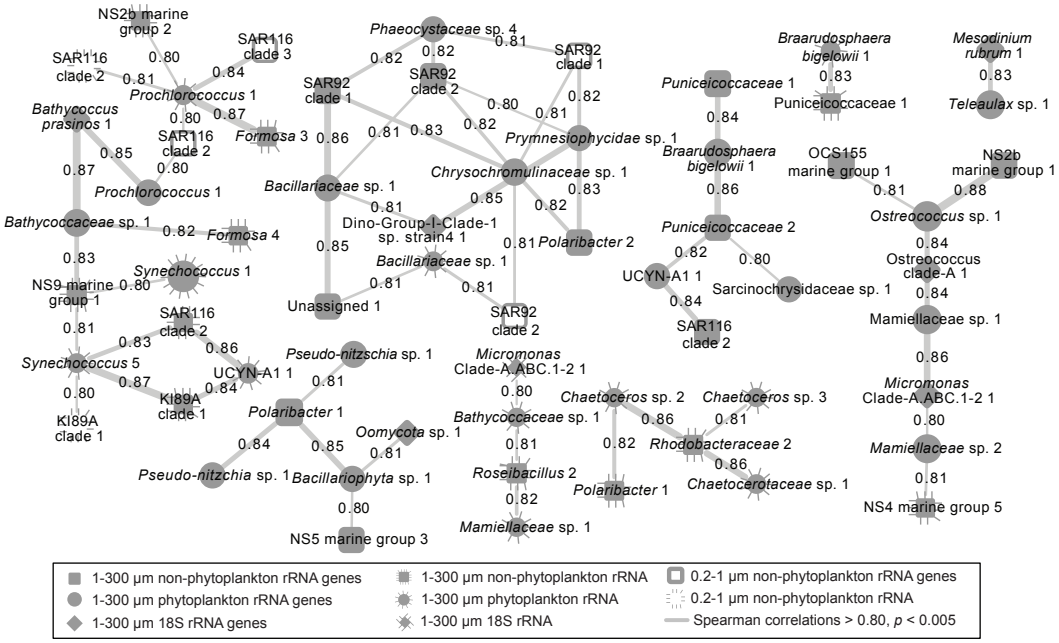

Figure 6 | Network showing pairwise positive correlations between phytoplankton and non-phytoplankton or *Eukaryota* rRNA and rRNA ASV or OTU relative proportions. As in Figure 4, nodes filled in with gray shading are from the 1-300 µm size fraction and those with no shading (open) are from the 0.2-1 µm size fraction. A dashed line surrounding a node indicates the node represents data from the rRNA sequence dataset, whereas a solid line or no-line indicates rRNA gene sequence dataset. Connecting lines indicate positive correlations (Spearman > 0.80, p & q < 0.001) and line thickness corresponds with strength of correlation. Only taxa with average relative abundance > 0.5% are shown.

Figure 7

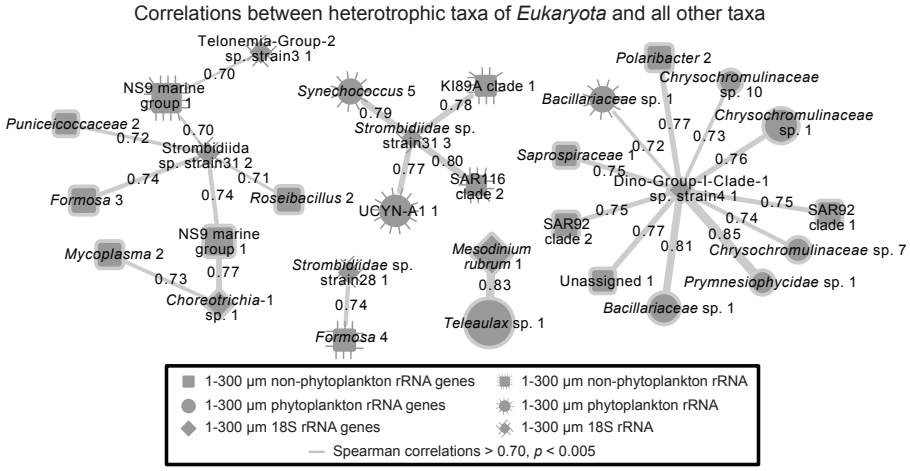

Figure 7 | Network showing pairwise positive correlations between heterotrophic *Eukaryota* to *Bacteria* and phytoplankton. Vertical lines surrounding a node indicates the node represents data from the rRNA sequence dataset, whereas no-line indicates rRNA gene sequence dataset. Lines connecting edges indicate correlations (Spearman > 0.70, p & q < 0.001; no correlations were observed < -0.70) and line thickness corresponds with strength of correlation. MAST heterotrophs would not show (see methods).

Figure 1

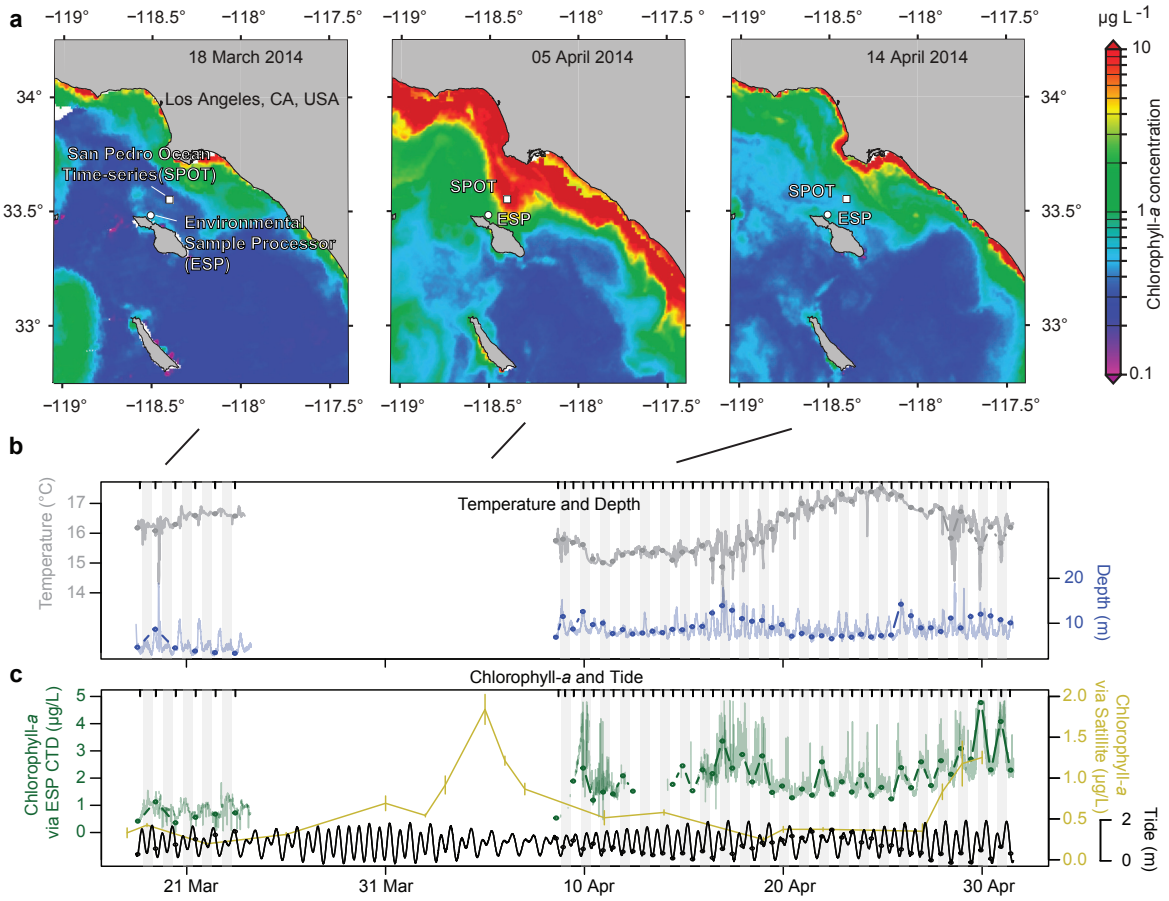

Figure 1 | Environmental context for the Environmental Sample Processor (ESP) deployment near Santa Catalina Island 18 Mar-1 May 2014. Sampling did not occur for about two weeks 23 Mar - 9 Apr due to ESP disconnection. Before the interruption, the microbial community was collected daily at 10:00, and, after, twice daily at 10:00 and 22:00. During the interruption, (**a**) satellite chlorophyll-*a* measurements indicated a small increase in chlorophyll-a occurred throughout the San Pedro Channel, peaking four days before resumption of sampling. (**b**) Temperature and depth, and (**c**) chlorophyll-*a* CTD ESP concentrations were measured every five minutes (the thin lines); chlorophyll-a data 12 – 15 April is missing due to poor quality. Satellite chlorophyll-a is the mean of 3-x-3 pixels (~ 3-x-3 km area) covering the region surrounding the ESP; the error bars are the standard deviation of the nine pixels used in calculation of the mean. Note, in these waters, the satellite-derived chlorophyll-a concentrations are generally representative of the upper 5 m of the water column, and the ESP was deployed between 5-20 m, so some variation in absolute concentration is expected. Tide data are observed water measurements for nearby Los Angeles, CA. Circles represent the average value during sample collection for microbial community analyses (usually about 30 minutes). (**b**) and (**c**) Sample collection times are indicated by ticks at the top of the figures.

Figure 2

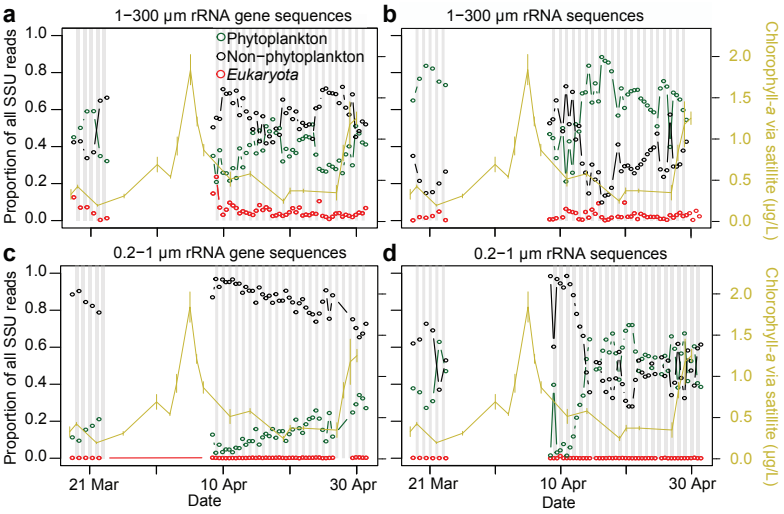

Figure 2 | Dynamics of the overall proportion of sequences observed using a single "universal" primer. The data was split into three partitions: "Phytoplankton" (green, chloroplast and cyanobacterial rRNA and rRNA gene sequences), "Non-Phytoplankton" (black, all remaining bacterial and archaeal 16S rRNA and rRNA gene sequences), and *Eukaryota* sequences (red, all 18S rRNA and rRNA gene sequences). Data are shown for the (**a**) 1-300 µm size fraction rRNA gene sequences, (**b**) 1-300 µm rRNA sequences, (**c**) 0.2-1 µm rRNA gene sequences, and (**d**) 0.2-1 µm rRNA sequences. Satellite chlorophyll-*a* concentrations and standard deviations (shown in yellow) are estimated by 3-x-3 pixels surrounding the ESP as in Figure 1.

Figure 3

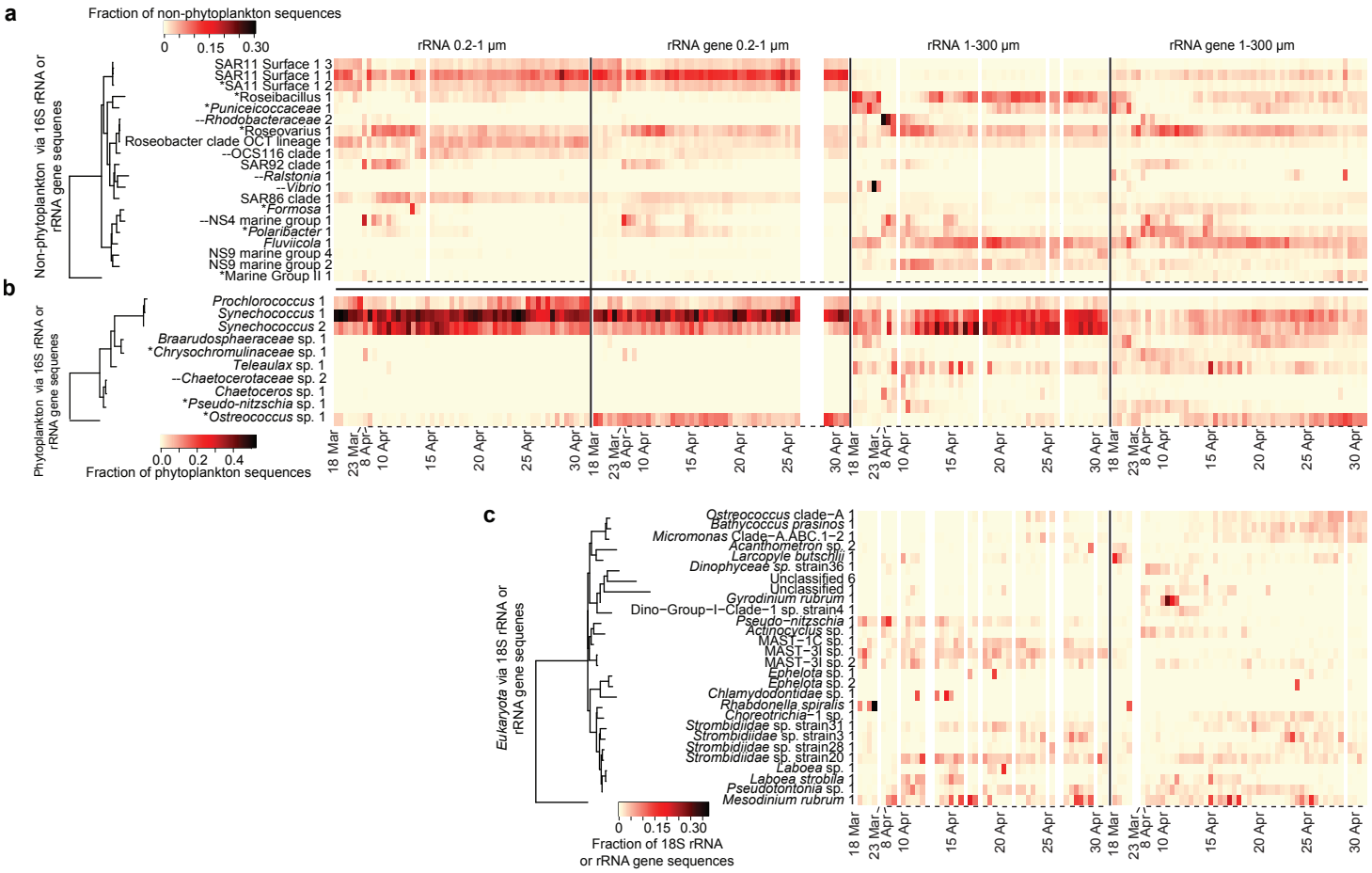

Figure 3 | Daily to semi-daily 16S and 18S rRNA and rRNA gene dynamics of microbial taxa. Heatmaps include data from (**a**) "non-phytoplankton" Bacteria and Archaea via 16S rRNA and rRNA gene sequences, (**b**) "phytoplankton", via 16S rRNA and rRNA gene sequences of chloroplasts and Cyanobacteria, and (**c**) *Eukaryota* taxa via 18S rRNA and rRNA gene, excluding metazoan sequences. Only ASVs or OTUs that ever became taxon with the highest proportion of sequences within a given dataset for at least one sample are shown. The tree shows the phylogenetic relatedness of the ASV or OTU according to the amplicon-sequenced region. Note that Mesodinium is known to have a very aberrant 18S rRNA gene sequence [49]. For the dates where two samples were taken per day (10:00 AM and 10:00 PM, 10 April - 1 May), a dash underneath a given sample indicates the sample was taken at night. All 16S rRNA and rRNA gene ASVs shown here were also detected during the 2011 diatom bloom study [7,10], except where "--" is found next to the ASV name; asterisks next to taxon names indicate that ASV was also found to most abundant during the 2011 study.

Figure 4

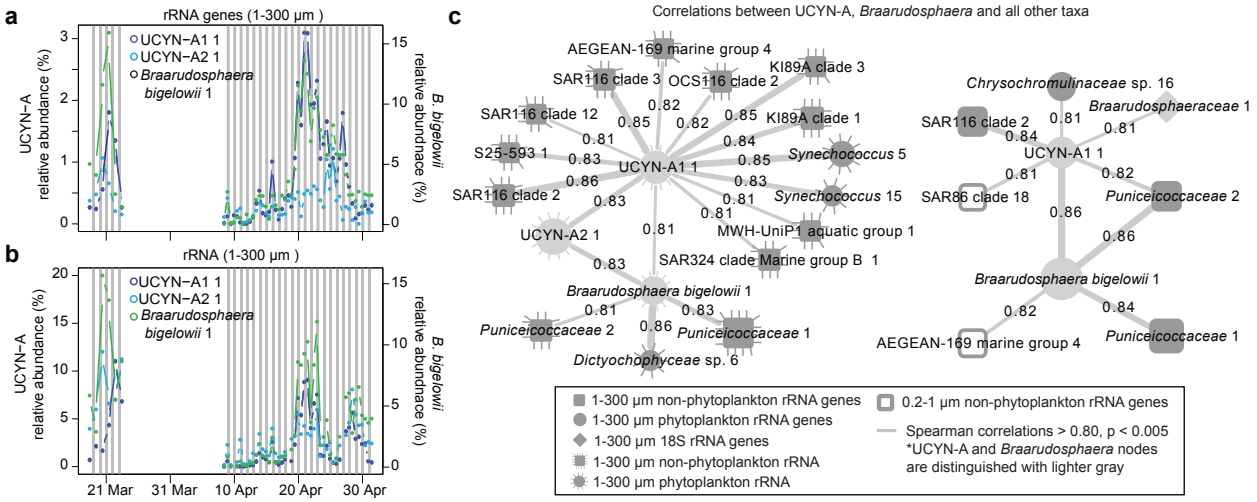

Figure 4 | Co-occurrence of symbionts UCYN-A and Braarudosphaera. Relative proportions are via 16S (**a**) rRNA genes and (**b**) rRNA as proportion of all phytoplankton chloroplasts and Cyanobacteria sequences in the 1-300 µm size fraction. (**c**) Co-occurrence network of taxa positively correlated to UCYN-A or *Braarudosphaera* taxa where circles, squares, and diamonds represent phytoplankton, non-phytoplankton, and Eukaryota rRNA and rRNA gene ASVs or OTUs, respectively. Nodes filled in with gray shading are from the 1-300 µm size fraction, and those with no shading (open) are from the 0.2-1 µm size fractions, respectively. Darker gray nodes indicate the UCYN-A and *Braarudosphaera* nodes. A dashed line surrounding a node indicates the node represents data from the rRNA dataset, whereas a solid line or no-line indicates rRNA gene. Lines connecting edges indicate positive correlations (Spearman $r > 0.80$, p & $q < 0.001$) and line thickness corresponds with strength of correlation.

Figure 5

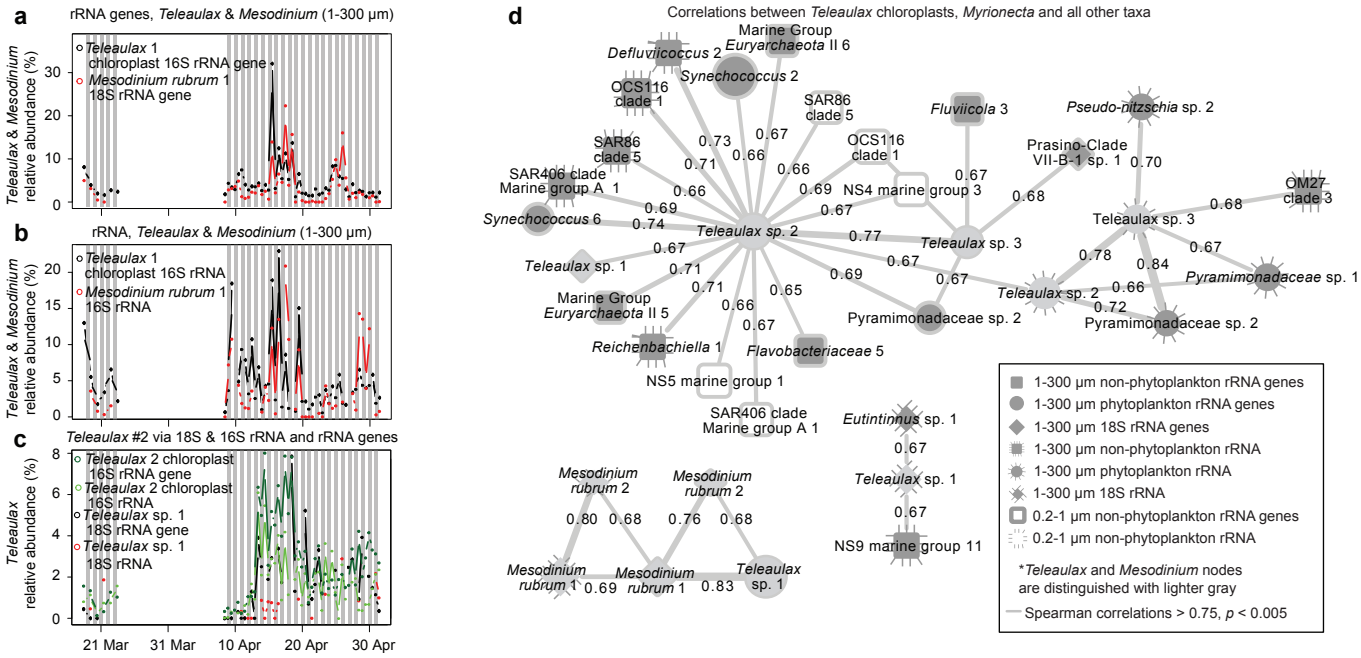

Figure 5 | Co-occurrence of symbionts of *Mesodinium rubrum* and *Teleaulax*. Dynamics of the dominant ASVs of *Mesodinium* and *Teleaulax* chloroplast via (**a**) rRNA gene sequences, and (**b**) rRNA sequences. Additionally, the dynamics of a (c) second Teleaulax chloroplast ASV and the Teleaulax with highest sequence proportions via 18S rRNA genes. (d) Co-occurrence network of taxa positively correlated to *Mesodinium* and *Teleaulax* showing that the dynamics of the apparent symbionts are not correlated to other taxa. Network colors and shapes are the same as in Figure 4.

Figure 6

Correlations between phytoplankton and all other taxa

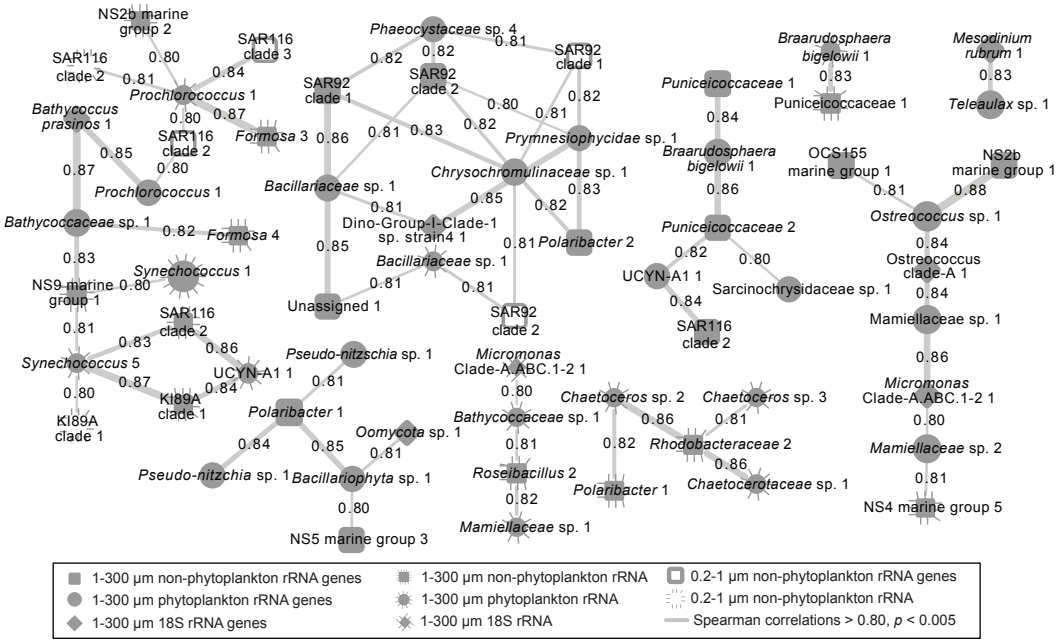

Figure 6 | Network showing pairwise positive correlations between phytoplankton and non-phytoplankton or *Eukaryota* rRNA and rRNA ASV or OTU relative proportions. As in Figure 4, nodes filled in with gray shading are from the 1-300 µm size fraction and those with no shading (open) are from the 0.2-1 µm size fraction. A dashed line surrounding a node indicates the node represents data from the rRNA sequence dataset, whereas a solid line or no-line indicates rRNA gene sequence dataset. Connecting lines indicate positive correlations (Spearman > 0.80, p & q < 0.001) and line thickness corresponds with strength of correlation. Only taxa with average relative abundance > 0.5% are shown.

Figure 7

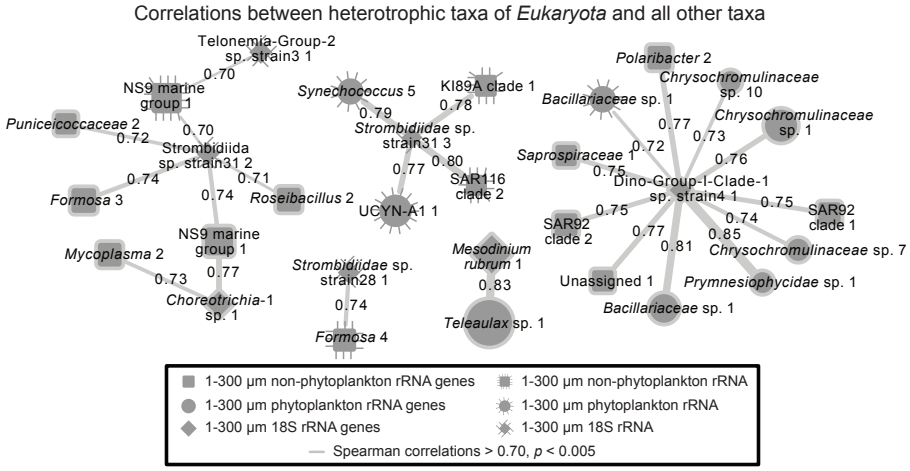

Figure 7 | Network showing pairwise positive correlations between heterotrophic *Eukaryota* to *Bacteria* and phytoplankton. Vertical lines surrounding a node indicates the node represents data from the rRNA sequence dataset, whereas no-line indicates rRNA gene sequence dataset. Lines connecting edges indicate correlations (Spearman > 0.70, p & q < 0.001; no correlations were observed < -0.70) and line thickness corresponds with strength of correlation. MAST heterotrophs would not show (see methods).